

**QUANTIFICATION OF CHAOTIC MIXING
IN MICROFLUIDIC SYSTEMS**

A Thesis

by

HO JUN KIM

Submitted to the Office of Graduate Studies of
Texas A&M University
in partial fulfillment of the requirements for the degree of

MASTER OF SCIENCE

August 2004

Major Subject: Mechanical Engineering

**QUANTIFICATION OF CHAOTIC MIXING
IN MICROFLUIDIC SYSTEMS**

A Thesis

by

HO JUN KIM

Submitted to Texas A&M University
in partial fulfillment of the requirements
for the degree of

MASTER OF SCIENCE

Approved as to style and content by:

Ali Beskok
(Chair of Committee)

Steve Suh
(Member)

Paul Cizmas
(Member)

Dennis O'Neal
(Head of Department)

August 2004

Major Subject: Mechanical Engineering

ABSTRACT

Quantification of Chaotic Mixing in Microfluidic Systems.

(August 2004)

Ho Jun Kim, B.S., Hanyang University

Chair of Advisory Committee: Dr. Ali Beskok

Periodic and chaotic dynamical systems follow deterministic equations such as Newton's laws of motion. To distinguish the difference between two systems, the initial conditions have an important role. Chaotic behaviors or dynamics are characterized by sensitivity to initial conditions. Mathematically, a chaotic system is defined as a system very sensitive to initial conditions. A small difference in initial conditions causes unpredictability in the final outcome. If error is measured from the initial state, the relative error grows exponentially. Prediction becomes impossible and finally, chaotic systems can come to become stochastic system.

To make chaotic motion, the number of variables in the system should be above three and there should be non-linear terms coupling several of the variables in the equation of motion. Phase space is defined as the space spanned by the coordinate and velocity vectors. In our case, mixing zone is phase space. With the above characteristics – the initial condition sensitivity of a chaotic system, our plan is to find most efficient chaotic stirrer. In this thesis, we present four methods to measure mixing state based on the chaotic dynamics theory.

The Lyapunov exponent is a measure of the sensitivity to initial conditions and can be used to calculate chaotic strength. We can decide the chaotic state with one real number and measure efficiency of the chaotic mixer and find the optimum frequency.

The Poincaré section method provides a means for viewing the phase space diagram so that the motion is observed periodically. To do this, the trajectory is sectioned at regular intervals. With the Poincaré section method, we can find 'islands' considered as bad mixed zones so that the mixing state can be measured qualitatively.

With the chaotic dynamics theory, the initial length of the interface can grow exponentially in a chaotic system. We will show the above characteristics of the chaotic system to prove as fact that our model is an efficient chaotic mixer.

The final goal for making chaotic stirrer is how to implement efficient dispersed particles. The box counting method is focused on measurement of the particles dispersing state. We use snap shots of the mixing process and with these snap shots, we devise a plan to measure particles' dispersing rate using the box-counting method.

TO MY PARENTS – Yong Soo Kim, Hyo Sook Lee
FOR THEIR LOVE AND SACRIFICES

ACKNOWLEDGMENTS

I would like to express my sincere gratitude to the people who have made this work possible. First, I appreciate my advisor, Prof. Ali Beskok, for his guidance and support. He has taken the time to teach me the concept of micro fluidics and to take care of me. Even though I have many shortcomings, he always tried to understand my situation and guide me. And he has been kind enough to share his knowledge not only about academics, but also other important things in life. It is my greatest fortune through all my life to meet Prof. Ali Beskok.

I thank Mr. Jungyoon Hahm and Mr. Pradip Kumar Bahukudumbi for their cooperation during my work at the laboratory. And I especially thank Pradip for his help in understanding my research work physically and experimentally.

I would like to express gratitude to my parents. They have been supporting me since I was born. Whenever I need their help, they always try to help me as much as possible even though they have their own difficulties. I will not forget their gratitude.

TABLE OF CONTENTS

| | Page |
|--|------|
| ABSTRACT..... | iii |
| DEDICATION..... | v |
| ACKNOWLEDGMENTS..... | vi |
| TABLE OF CONTENTS..... | vii |
| LIST OF TABLES..... | ix |
| LIST OF FIGURES..... | x |
| CHAPTER | |
| I INTRODUCTION..... | 1 |
| 1.1 Introduction..... | 1 |
| 1.2 Purpose of research..... | 2 |
| 1.3 Organization of thesis..... | 3 |
| II LITERATURE REVIEW..... | 5 |
| 2.1 Chaotic mixing model..... | 5 |
| III LYAPUNOV EXPONENT AND SENSITIVITY TO INITIAL CONDITION..... | 9 |
| 3.1 Sensitivity to the initial condition in chaotic state..... | 9 |
| 3.2 Calculation of the Lyapunov exponent..... | 15 |
| IV POINCARÉ SECTION..... | 20 |
| 4.1 Usefulness of Poincaré section in chaotic dynamics..... | 20 |
| 4.2 Poincaré section and destruction of islands..... | 25 |

| CHAPTER | Page |
|--|------|
| V STRETCHING OF INTERFACE..... | 38 |
| 5.1 Definition of stretching of interface..... | 38 |
| 5.2 Stretching ratio and Lyapunov exponent..... | 48 |
| 5.3 Line stretching and hyperbolic fixed points..... | 51 |
| VI PARTICLE SPREAD..... | 54 |
| 6.1 Definition of box counting method..... | 54 |
| 6.2 How to calculate mixing index..... | 56 |
| VII CONCLUSIONS AND FUTURE WORK..... | 80 |
| REFERENCES..... | 82 |
| VITA..... | 85 |

LIST OF TABLES

| TABLE | | Page |
|-------|---|------|
| 3-1. | FTLE values for various patterns at $T=4, 6, 8$ | 19 |

LIST OF FIGURES

| FIGURE | | Page |
|--------|--|------|
| 2-1. | Qian and Bau's flow patterns, adopted from [5]..... | 6 |
| 2-2. | Qian and Bau's chaotic mixing model [5]. Electrode surfaces and the corresponding slip velocity directions are shown..... | 7 |
| 3-1. | Ling et al's model [9]..... | 10 |
| 3-2. | Flow patterns from Ling et.al [9]..... | 10 |
| 3-3. | Deformation of blob in the center of a non-chaotic mixer. The right figure is obtained at non-dimensional time $t=50$ | 11 |
| 3-4. | Deformation of a blob in the center zone of a chaotic mixer. The right figure is obtained at non-dimensional time $t=50$ | 12 |
| 3-5. | Dispersed particles with chaotic advection. Right figure is obtained at time $t=50$ | 13 |
| 3-6. | Schematics for calculating the Lyapunov exponent using Sprott's method..... | 15 |
| 3-7. | FTLE exponents for pattern B- C at time periods of $T = 4, 6, 8$ | 18 |
| 3-8. | FTLE at different initial conditions converge to the same value for pattern B-C at $T=6$ | 18 |
| 4-1. | Understanding of limit cycle in three dimensional phase space..... | 21 |
| 4-2. | Poincaré section of a three-dimensional orbit..... | 22 |
| 4-3. | Poincaré section of periodic points. Left figure shows a single period, while right figure shows two periodic points [4]..... | 23 |
| 4-4. | Poincaré section of 2-dimensional unsteady case [4]..... | 24 |
| 4-5. | Pattern A and B ; $T=6.0$; 121 particles ; 100 periods..... | 27 |
| 4-6. | Pattern A and C ; $T=6.0$; 121 particles ; 100 periods..... | 27 |
| 4-7. | Pattern A and D ; $T=6.0$; 121 particles ; 100 periods..... | 27 |

| FIGURE | Page |
|--|------|
| 4-8. Pattern B and C ; T=6.0 ; 121 particles ; 100 periods..... | 28 |
| 4-9. Pattern B and D ; T=6.0 ; 121 particles ; 100 periods..... | 28 |
| 4-10. Pattern C and D ; T=6.0 ; 121 particles ; 100 periods..... | 28 |
| 4-11. Pattern B and C ; 121 particles ; 100 periods ; T = 1.0, 2.0, 3.0, 4.0, 6.0 We fixed pattern pair as B-C pattern and change the period size to check destruction of KAM boundaries..... | 29 |
| 4-12. Pattern B and C ; 20 particles ; 300 periods ; T = 1.0, 1.5, 2.0, 2.5, 3.0, 6.0..... | 32 |
| 4-13. Islands @ Pattern B and C ; T = 1.0, 1.5..... | 34 |
| 4-14. Islands @ Pattern B and C ; T = 2.0, 2.5..... | 35 |
| 4-15. Islands @ Pattern B and C ; T = 3.0, 6.0..... | 36 |
| 5-1. Line of particles..... | 38 |
| 5-2. Interface stretching evolution : B and C pattern T=6.0 case, with 10000 particles..... | 39 |
| 5-3. Interface stretching with 100 particles for various cases..... | 43 |
| 5-4. Comparison between B and C pattern T=4.0 case and T=6.0 case (100 particles case)..... | 43 |
| 5-5. Stretching values are saturated after 50 nondimensional time because mixing zone is closed space (100 particles case)..... | 44 |
| 5-6. Exponential growth of stretching ratio with 1000 particles..... | 44 |
| 5-7. Exponential growth of stretching ratio with (a) 100, (b) 1000 particles. Although the number of particles is different for each case, order of growth of stretching ratio is similar..... | 45 |
| 5-8. Different saturation points-B and C pattern (100, 1000 particles)..... | 46 |
| 5-9. Snap shots of stretching of interface (B and C pattern , size of T = 4.0 , 1000 particles)..... | 47 |

| FIGURE | Page | |
|--------|--|----|
| 5-10. | Exponential growth of interface stretching : With increasing number of particles, the stretching exponent increases..... | 49 |
| 5-11. | Exponential growth of interface stretching with 100 particles: this graph shows relation between Lyapunov exponent and stretching exponent..... | 50 |
| 5-12. | We can find relation between converged Lyapunov exponent and converged value of stretching..... | 50 |
| 5-13. | Snap shots of stretching of interface (B and C pattern , size of T = 6, 500 particles..... | 52 |
| 5-14. | Stretching Ratio : The order of stretching ratio follows the order of Lyapunov exponent..... | 53 |
| 5-15. | Positions of hyperbolic fixed points..... | 53 |
| 6-1. | Particles located in cells..... | 57 |
| 6-2. | Size of cell for 40,000 particles case..... | 58 |
| 6-3. | Coarse selection of box size..... | 59 |
| 6-4. | Steady case , 10000 particles ; T=10.0..... | 60 |
| 6-5. | T=10.0, 20000 particles..... | 61 |
| 6-6. | T=11.0, 10000 particles..... | 62 |
| 6-7. | Comparison of mixing index :Gradient symbol : steady case (regular stirring), Diamond symbol : unsteady case, T=10.0 (chaotic stirring), Triangular symbol : unsteady case, T=11.0 (chaotic stirring)..... | 63 |
| 6-8. | Snap shots of deformation of blob A and D pattern : size of T = 6.0, 1600 particles..... | 66 |
| 6-9. | A and D pattern, size of T = 6.0 , 1600 particles without concern of number of particles per box..... | 68 |
| 6-10. | A and D pattern, size of T = 6.0 , 1600 particles with concern of number of particles per box..... | 68 |

| FIGURE | Page |
|---|------|
| 6-11. Snap shots of deformation of blob B and C pattern : size of T = 6.0, 1600 particles..... | 69 |
| 6-12. B and C pattern , size of T = 6.0 , 1600 particles without concern of number of particles per box..... | 71 |
| 6-13. B and C pattern , size of T = 6.0 , 1600 particles with concern of number of particles per box..... | 71 |
| 6-14. Snap shots of deformation of blob B and C pattern , size of T = 8.0 , 1600 particles..... | 72 |
| 6-15. B and C pattern , size of T = 8.0 , 1600 particles MI without concern of number of particles per box..... | 74 |
| 6-16. B and C pattern , size of T = 8.0 , 1600 particles MI without concern of number of particles per box..... | 74 |
| 6-17. Comparison of Mixing Index between “B and C” and “A and D” (1-og - linear scale) : Without concern of number of particles per box, T = 6.0 fixed..... | 75 |
| 6-18. Comparison of Mixing Index between “B and C” and “A and D” (1-og - linear scale) : With concern of number of particles per box, T = 6.0..... | 75 |
| 6-19. Comparison of Mixing Index between “B and C” T=6.0 and T=8.0 (log - linear scale) : Without concern of number of particles per box | 76 |
| 6-20. Comparison of Mixing Index between “B and C” T=6.0 and T=8.0 (log - linear scale) : Without concern of number of particles per box | 76 |
| 6-21. B and C pattern : size of T = 6.0, 10000 particles..... | 77 |
| 6-22. Mixing Index..... | 79 |

CHAPTER I

INTRODUCTION

1.1. INTRODUCTION

Flow and species transport in micro-scales experience laminar, even Stokes flow conditions. In absence of turbulence, species mixing in micro-scales becomes inherently diffusion dominated, and requires very long mixing lengths and large time-scales. This creates significant challenges in design of efficient mixers for microfluidic devices, such as micro-total-analysis-systems utilized in detection of biological and chemical agents for medical, pharmaceutical and homeland security applications. Although majority of the previous research concentrated on enhancement of diffusive-mixing by increasing the interspecies contact area, recent work focuses on inducing chaotic advection, which is a conceivable method for species mixing enhancement even in the Stokes flow regime [1, 2].

In general, for two-dimensional unsteady and three-dimensional steady flows, fluid-particle trajectories obtained using the Lagrangian description of motion can not be integrated analytically, and the particle trajectories exhibit chaotic trends. This result in advection of the particles to a larger portion of the flow domain, and the stretching rate between groups of particles may become exponential, resulting in efficient mixing. These

This thesis follows the style and format of *Analytical Chemistry*.

characteristics can not be observed for non-chaotic (integrable) flows.

Micro-scale species mixing using chaotic advection is becoming a focal point in microfluidics. Recently, Stroock *et al.* [3] has utilized steady Stokes flow in a rectangular micro-channel with staggered herringbone-shaped grooved bottom – surface [2]. This geometry imposed alternating secondary flow patterns, resulting in spatially evolving three-dimensional *steady* Stokes flow. Experiments utilized confocal laser scanning microscopy based laser-induced-fluorescence measurements. Standard deviation of the fluorescence intensity in confocal images, as a function of the downstream distance is utilized to determine the mixer efficiency. Chaotic advection resulted in orders of magnitude reduction in the mixing length, compared to the diffusive mixing. Qian and Bau have theoretically investigated chaotic advection in electroosmotically driven micro-mixer under time-periodic variations of the wall zeta potential [3]. Such alterations of the zeta potential can be achieved using surface imbedded electrodes.

1. 2. PURPOSE OF RESEARCH

The purpose of our research is to quantify the mixing efficiency in a chaotic microfluidic system using the following approaches:

1. Lyapunov Exponent: Exponent of the rate of stretching between two adjacent particles [4].
2. Poincaré Section: Superposition of stroboscopic images of particles captured at specified periods [4].

3. Interface Stretching Rate: The rate of increase of the interface length by time [5]
4. Mixing Index: Calculated using the position of dispersed particles [6].

The first method requires detailed knowledge about the flow field, and it is computationally expensive. It requires high-resolution numerical solutions, which is in general difficult to obtain using low-order numerical discretizations. Numerical requirements of other methods are not as stringent as the computation of Lyapunov exponents. In fact, the numerical complexity is reduced as one goes down the list above. Therefore, it is desirable to develop a comprehensive understanding between the behaviors of these various tests. For example, without very detailed analysis of a computational mixing simulation, one should be able to state the quality of mixing and decide whether the flow is chaotic or not.

Motivated by this objective, we plan to utilize Qian and Bau's "Chaotic Electroosmotic Stirrer" design [5], and test this system under different combinations of flow patterns and frequencies, and correlate the outcomes of various tests in a comprehensive manner.

1.3. ORGANIZATION OF THESIS

This thesis is organized as follows: In Chapter II, Qian and Bau's chaotic mixing model is reviewed. Chapter III presents concept of finite time Lyapunov exponent and we calculate Lyapunov exponent for all possible flow pattern pairs, and compare the converged Lyapunov exponent values to find the best mixing conditions. Chapter IV explains the Poincaré section concept, and we show Poincaré sections for various cases, including the

KAM boundaries, which result in poor mixing zones. In Chapter V, we examine the growth of a fluid interface, exponential growth in chaotic states are demonstrated. In Chapter VI, we introduce the box counting method, and define a mixing index to quantify the mixing efficiency. Finally, in Chapter VII, we conclude and state the future research directions.

CHAPTER II

LITERATURE REVIEW

2.1 CHAOTIC MIXING MODEL

In this section, we briefly present a design that induce chaotic mixing using two-dimensional, time-periodic electroosmotic flows, developed by Qian and Bau [5]. Electroosmosis is the process of inducing motion of ionized liquid relative to the stationary charged surfaces using applied electric fields. It is an effective mechanism to drive micro-flows without any mechanical pumping components. Since electroosmosis is driven by the electric fields, rapid switching between several different electric field configurations and/or temporally varying the surface zeta-potentials create different flow fields, susceptible to chaotic advection and mixing. Therefore, electroosmosis enables fast flow response, limited only by the flow development time-scales [7].

Qian and Bau [5] investigated chaotic advection theoretically in an electroosmotically driven micro-mixer, under time-periodic variations of the wall zeta potential, which can be achieved using surface imbedded electrodes [5]. Figure 2-1 shows the mixer that consists of a rectangular box with four zeta-potential patterned surfaces on its top and bottom surfaces. The left and right walls are electrodes, and they induce a uniform electric field. Depending on the magnitude and the sign of the surface zeta potential, a uniform slip-velocity is generated on the surface. Qian and Bau obtained the velocity field

by solving the Stokes equations subject to various wall slip-velocities. Details of their analytical solution and the electrokinetic flow theory will be presented in this thesis. Figure 2-1 also shows various flow patterns developed by selectively altering the surface zeta-potential. Figure 2-2 shows the direction of the electric field and the corresponding electroosmotic slip velocity on electrode surfaces.

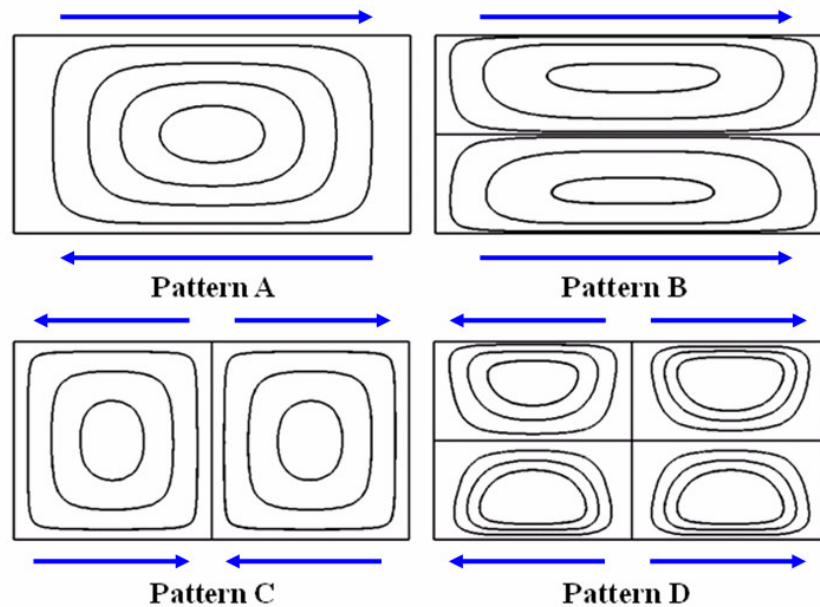


Figure 2-1. Qian and Bau's flow patterns, adapted from [5].

A time-periodic flow, with period T , can be generated by switching between any two flow-patterns with half period time-scales. We utilized various combinations of patterns A, B, C, and D, to form time-periodic electroosmotic flows, and we varied the time-period from $T=1.0$ to 8.0 (in convective time-scale units).

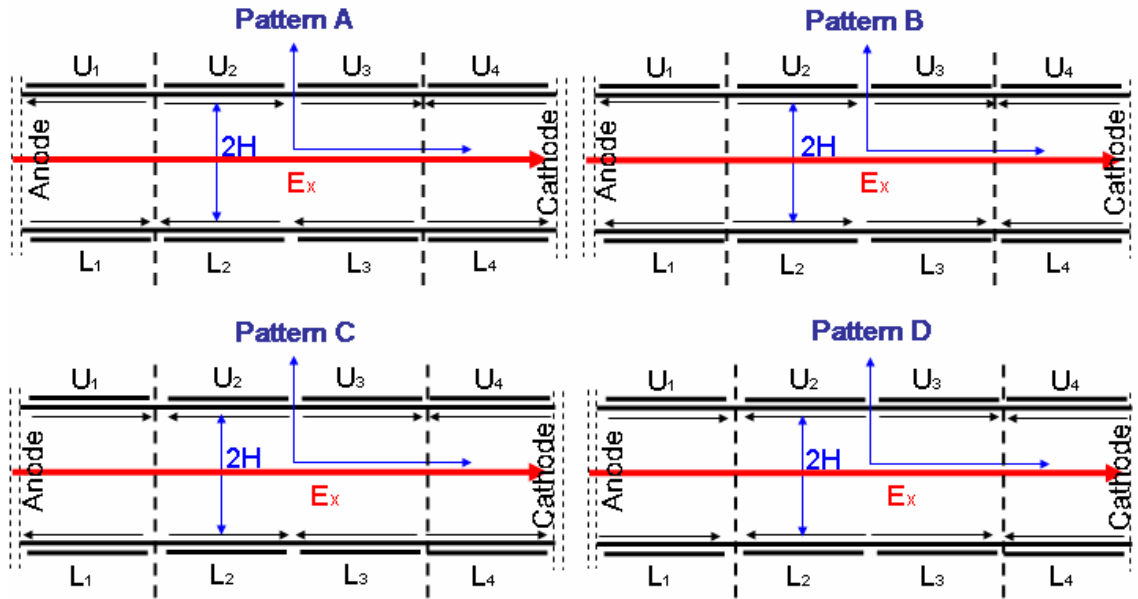


Figure 2-2. Qian and Bau's chaotic mixing model [5]. Electrode surfaces and the corresponding slip velocity directions are shown

Qian and Bau modeled the flow using the dimensionless Stokes equation.

$$\text{Re} \frac{\partial \vec{V}}{\partial t} = -\nabla p + \nabla^2 \vec{V} \quad (2.1)$$

In the above, $\vec{V} = \{U, V\}$ is the velocity vector, U and V are the velocity components in the X and Y directions, respectively; p is the pressure; and t is the time, and Re is the Reynolds number. Equation (2.1) is non-dimensionalized using the fluid kinematic viscosity, electroosmotic slip velocity, and the conduit's half-height, H .

In their analysis, Qian and Bau assumed that the gap between any adjacent electrodes is large compared to the electric double layer thickness (EDL), but it is small compared to H . Hence for mathematical simplicity, they neglected the gap between the

adjacent electrodes. They also demonstrated that when the gap is relatively small compared to H , it has no significant effect on the flow pattern.

By imposing potential differences between the embedded electrodes covered with thin insulating material alters the zeta potential (See Figure 2-2) [5]. In addition, they assume that such modulations in the charge distribution on the insulated electrodes do not affect the external electric field, E_x . The external electric field interacts with the mobile charges in the EDL, to generate fluid motion [5]. The charge polarity (positive or negative) dictates the direction of the fluid motion. To the first approximation, the velocity in the wall's vicinity can be approximated with the 'Helmholtz–Smoluchowski' electroosmotic slip velocity

$$V_{HD} = -\frac{\zeta \epsilon E_x}{\mu} . \quad (2.2)$$

We must emphasize that $Re \ll 1$ in Stokes flows, since all the terms in equation (2.1) balance each other, the flow transients represented by the time derivative term in equation (2.1) is indeed very fast (since for $Re \rightarrow 0$, $\partial V / \partial t \rightarrow \infty$). This enabled Qian and Bau to neglect the flow transients, as they switch between the various flow solutions [5].

CHAPTER III

LYAPUNOV EXPONENT AND SENSITIVITY TO INITIAL CONDITION

Sensitivity to the initial condition is a signature of chaos. For chaotic systems, time evolution of initially close two particles exhibit exponential divergence. This means that in chaotic systems, the position of two initially nearby particles (say 10^{-6} H apart) will be extremely different after a certain time. In this chapter, we introduce the Lyapunov exponent as a measure of chaotic strength.

3.1 SENSITIVITY TO THE INITIAL CONDITION IN CHAOTIC STATE

Lyapunov exponents are the average exponential rate of divergence or convergence of nearby orbits in phase space. Since the nearby orbits correspond to nearly identical states, exponential orbital divergence means that for systems whose initial differences we may not be able to initially resolve will soon behave quite differently [8]. This sensitivity to initial conditions is the main characteristic of chaotic systems, and chaotic motion of fluid particles increases the mixing efficiency by enhancing the dispersion of passive particles. As we know, Lyapunov exponent is used to measures the rate of exponential divergence of two initially near by trajectories.

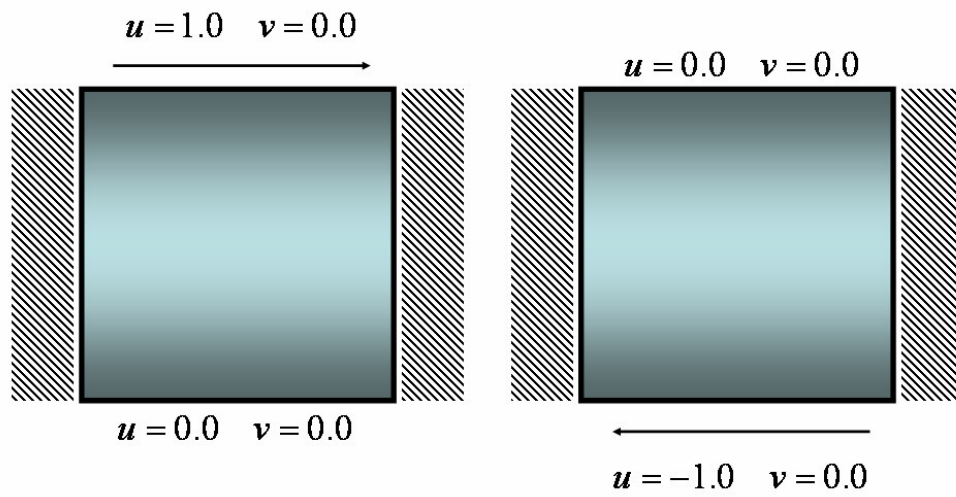
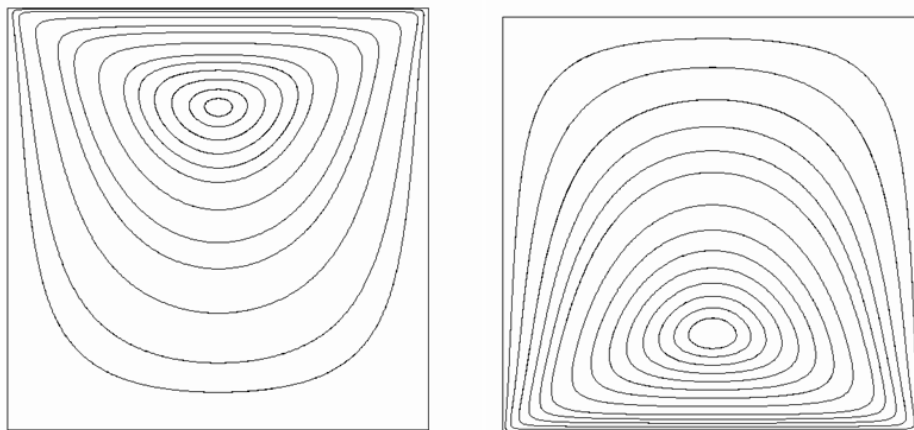


Figure 3-1. Ling et al's model [9]

Figure 3-2. Flow patterns from Ling *et al* [9]

We first refer to Ling et al's model to explain sensitivity to the initial conditions. The model consists of combinations of two different shear-driven cavity problems shown in Figure 3-1 [9]. The flow patterns obtained by shearing the top and bottom cavity surfaces are shown in Figure 3-2 [9]. Assuming fast transients for unsteady Stokes flows enable alternating the flow field between patterns 1 and 2, which results in chaotic advection.

Let's observe dispersion of nearby particles for the steady and time-periodic flows, where the time-periodic flow oscillates between the two flow patterns shown in Figure 3-2. We initially put 10,000 passive particles in the center of the mixing zone and observe their motion. Figure 3-3 shows that deformation of the blob in the center zone is regularly shaped for steady flow. This corresponds to the non-chaotic system. In the non-chaotic state, the distance between initially adjacent two particles does not change substantially, so that the non-chaotic system is insensitive to the initial conditions.

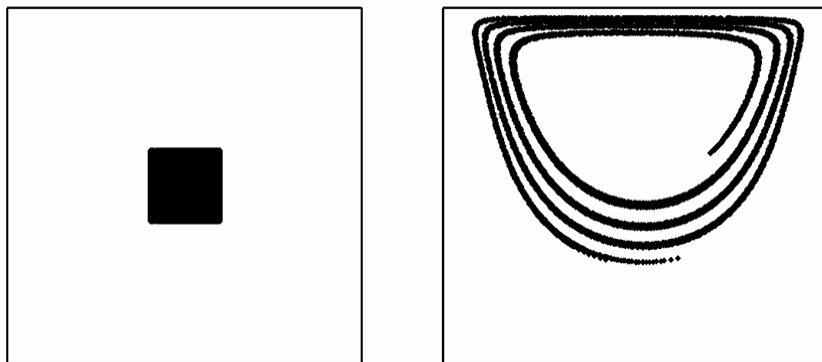


Figure 3-3. Deformation of blob in the center of a non-chaotic mixer. The right figure is obtained at non-dimensional time $t=50$

When we employ time-periodic Stokes flow alternating between the patterns shown in Figure 3-2, we observe that the blob initially in the middle of the mixing section

disperses randomly (See Figure 3-4). Snapshots of particle locations at time $t=50$ is shown in both figures. Mixing/dispersion of particles are significantly different in steady versus time-periodic flow.

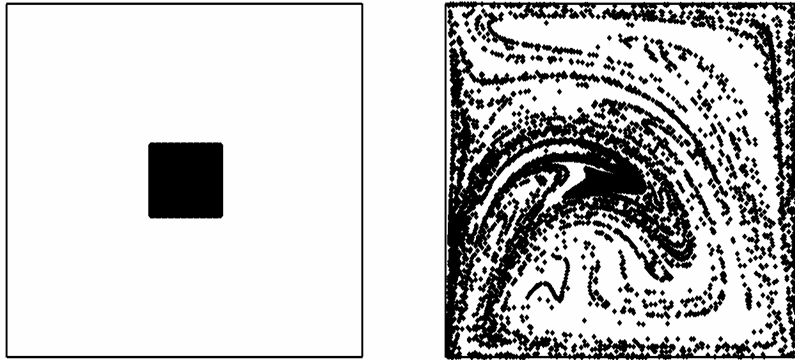


Figure 3-4. Deformation of a blob in the center zone of a chaotic mixer. The right figure is obtained at non-dimensional time $t=50$

In Figure 3-5, we show time evolution of three groups of particles for chaotic flow. In each group, we employed 100 particles, and located these particles in circle, by keeping 1^{-6} distance between adjacent particles. At time $t=50$, we observe that the initially concentrated particles are dispersed to the whole mixing zone. This shows sensitivity of a chaotic system to the initial conditions.

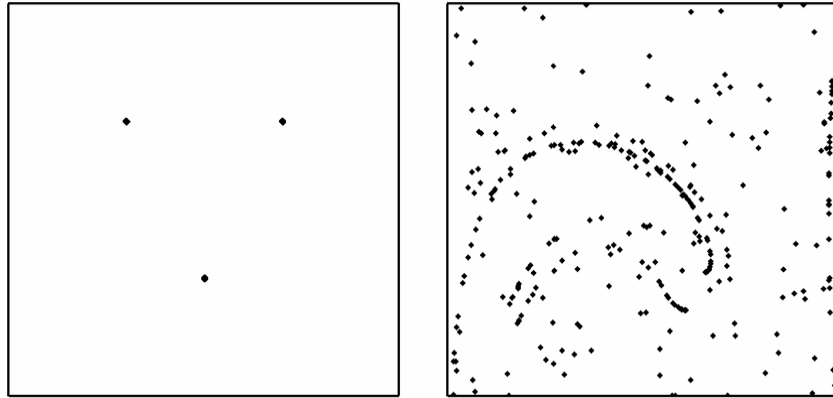


Figure 3-5. Dispersed particles with chaotic advection. Right figure is obtained at time $t=50$

The calculation of the largest Lyapunov exponent can be used to represent the chaotic strength. Hence, the Lyapunov exponent can be used to quantify the mixing efficiency. According to the theory of nonlinear dynamics, the largest Lyapunov exponent should be positive in the chaotic state, where the Lyapunov exponent is defined as

$$\lambda = \lim_{t \rightarrow \infty} \frac{1}{t} \ln |m_i(t)| = \lim_{t \rightarrow \infty} \left[\frac{1}{t} \ln \left(\frac{|dx(t)|}{|dx(0)|} \right) \right] \quad i = 1, \dots, n \quad (3.1)$$

where $m_1(t)$, $m_2(t)$ to $m_n(t)$ are the Eigenvalues of the fundamental solution matrix

$\Phi_t(x_0)$, satisfying

$$\dot{\Phi}_t = Df(x, t) \Phi,$$

where Φ means solution of flow equation, D means differentiation, x means current position, t means current time. Therefore, Lyapunov exponent is a generalization of the Eigenvalues at an equilibrium point [10].

$$\lambda = \lim_{t \rightarrow \infty} \frac{1}{n\Delta t} \sum \ln \left(\frac{|dx'((n+1)\Delta t)|}{|dx(n\Delta t)|} \right) \quad (3.2)$$

This definition is used for the discrete systems. Our research will be focused on numerical calculations of the Lyapunov exponents, where we try to determine the time period T , which will result in optimum mixing state.

3.2 CALCULATION OF THE LYAPUNOV EXPONENT

We utilized Sprott's method to calculate the Lyapunov exponents [11]. This method uses the general idea of following two nearby orbits, and calculates average logarithmic rate of separation of the two orbits. Whenever the orbits get too far apart, a new orbit in the vicinity of one of the orbits is chosen. A conservative procedure is to do this at each time-step, as shown in [11]. The numerical procedure is demonstrated in Figure 3-6.

$d_0 =$ *initial distance of nearby particle (virtual particle)*

$d_1 =$ *next time step's distance of nearby particle (virtual particle)*

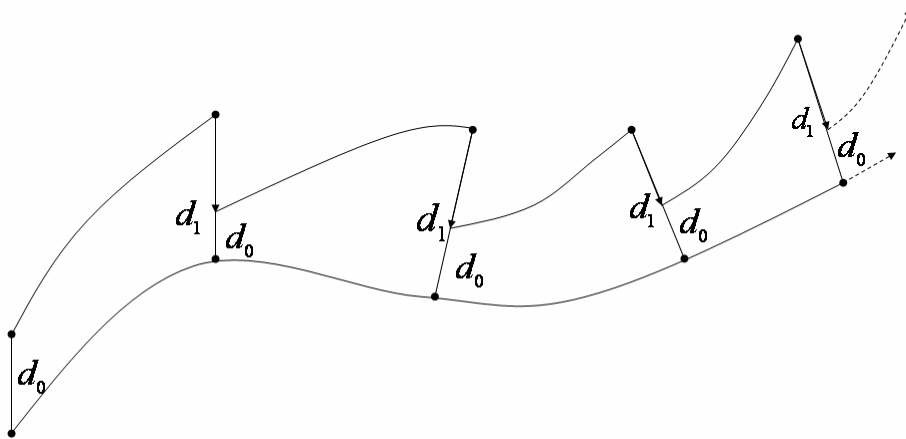


Figure 3-6. Schematic for calculating the Lyapunov exponent using Sprott's method [11]

We can choose any initial point to track the path of the main particle and to calculate the Lyapunov exponent in the mixing zone [8, 11, 12]. At the same time, initial position of the virtual (nearby) particle is used to evaluate the distance change between the virtual and

main particles. We then choose the number of time periods that we would calculate the Lyapunov exponent. Only when the number of period is sufficiently chosen, the Lyapunov exponent can be converged and in other words, the particle can move towards an attractor [8, 11, 12]. Then, we decide on size of the initial particle separation d_0 . This must be done by considering the machine precision. A proper choice for d_0 should be above 1000 times of the floating point precision that are being used [8, 11].

The algorithm is as follows. We advance both orbits for one iteration and calculate the new separation distance d_1 by sum of the squares of the differences in each space variable. For example, for a 2-dimensional system with variables x and y , the separation would be

$$d = \left[(x_1 - x_0)^2 + (y_1 - y_0)^2 \right]^{\frac{1}{2}} \quad (3.3)$$

where the subscripts denote the two orbits, 0 and 1 denoting the virtual and main particles, respectively. Then we select the new position of the virtual particle and size of d_0 in next time step. Selection of position is very important for convergence of the Lyapunov exponent in time. The new position of the virtual particle should be located between the main particle and position of the previous virtual particle (See Figure 3-6). Probably, this is the most difficult and error-prone step in the algorithm. We then find the logarithm of the separation rate, and perform averaging, as described in equation (3.2) [8, 11, 12]. This procedure is known as the Finite Time Lyapunov Exponent (FTLE).

Using these four flow patterns for half a period ($T/2$) each, we obtain six different

pattern combinations (A-B, A-C, A-D, B-C, B-D, and C-D). Figure 3-6 shows time evolution of the Lyapunov exponent for various time periods. We computed the Finite Time Lyapunov Exponent (FTLE) for all of these patterns for non-dimensional periods of $T=4$, 6 and 8, where T is normalized by the convective time-scale (based in the half channel height and the electroosmotic slip velocity from equation (2.2)). Variation of the FTLE as a function of time for $T=4$, 6, and 8 cases are shown in Figure 3.6. For all the cases, the initial particle location was at $(x,y)=(0.5,0.1)$, and the virtual particles was initially offset by 10^{-5} . The results have shown that the pattern B-C at $T=6.0$ has the largest FTLE, $\lambda_F = 0.308$. While, for $T=8.0$, $\lambda_F = 0.199$ and $T=4.0$, $\lambda_F = 0.251$ are obtained, respectively. Figure 3.7 shows FTLE obtained for pattern B-C at $T=6$ using three different initial conditions. The FTLE converged to the same value, as shown in the figure. The FTLE values for other flow patterns and time periods are given in Table 3-1. We observe from Table 3-1 that the FTLE for pattern B-C, at $T=6.0$ case is the largest, one among various cases studied here. Therefore, we expect this case to be the best mixing case. We must add here that for some pattern combinations islands of bad mixing zones are observed, and FTLE at these locations are $\lambda_F \approx 0$. Therefore, particular attention should be paid to such bad mixing zones, and Poincaré section method described in the next chapter can be used to determine the effects of these bad mixing zones.

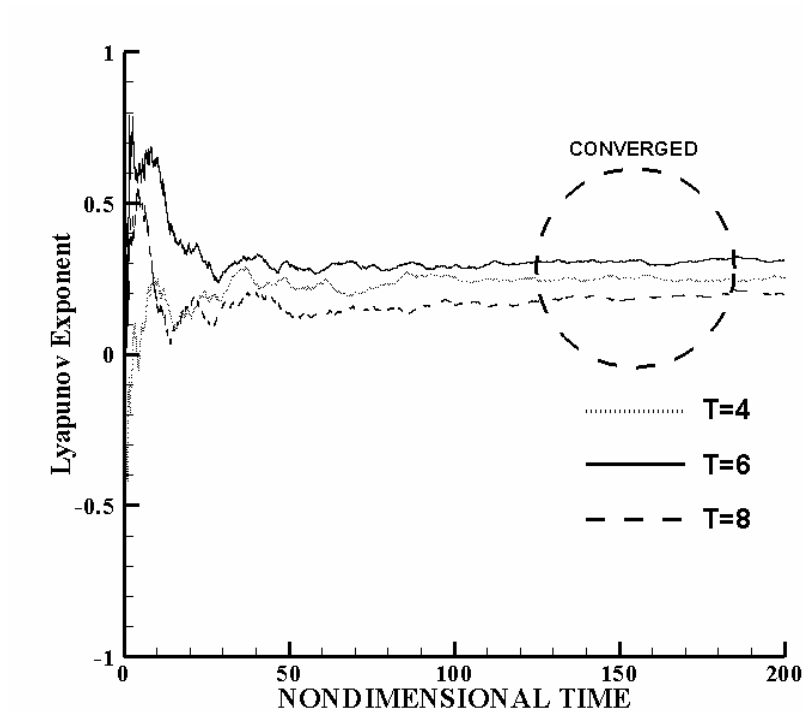


Figure 3-7. FTLE exponents for pattern B- C at time periods of $T = 4, 6, 8$

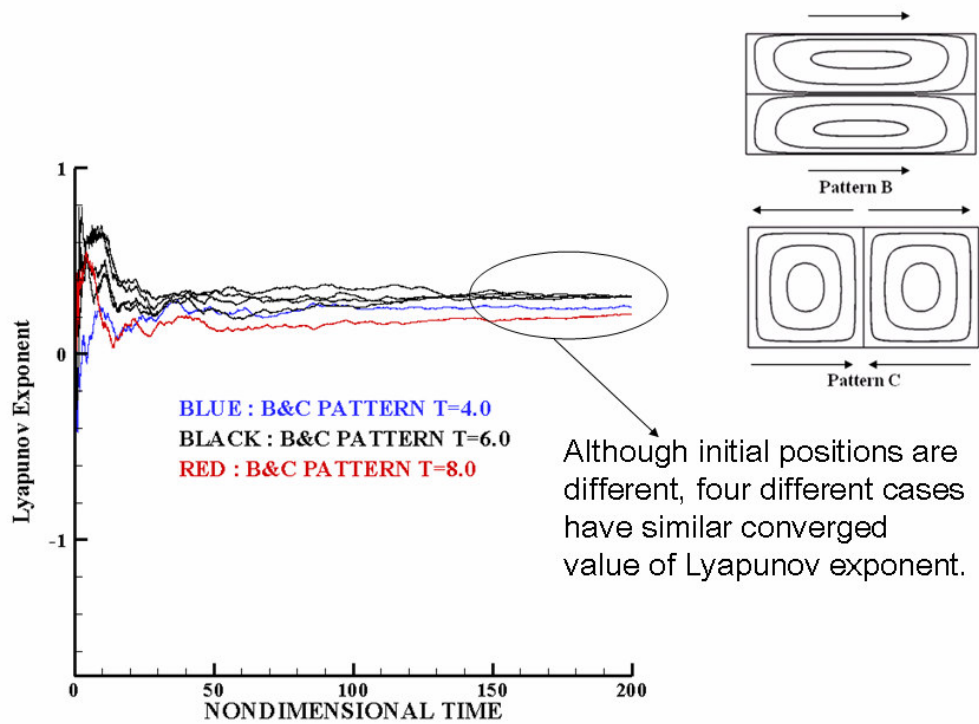


Figure 3-8. FTLE at different initial conditions converge to the same value

Table 3-1. FTLE values for various patterns at T=4, 6, 8

| A and B | |
|------------------|--------------------------|
| size of T | Lyapunov Exponent |
| | |
| 4.0 | -0.00019 |
| 6.0 | 0.01202 |
| 8.0 | 0.03360 |

| B and C | |
|------------------|--------------------------|
| size of T | Lyapunov Exponent |
| | |
| 4.0 | 0.25148 |
| 6.0 | 0.31084 |
| 8.0 | 0.19925 |

| A and C | |
|------------------|--------------------------|
| size of T | Lyapunov Exponent |
| | |
| 4.0 | 0.16289 |
| 6.0 | 0.10881 |
| 8.0 | 0.06122 |

| B and D | |
|------------------|--------------------------|
| size of T | Lyapunov Exponent |
| | |
| 4.0 | 0.18838 |
| 6.0 | 0.18313 |
| 8.0 | 0.16869 |

| A and D | |
|------------------|--------------------------|
| size of T | Lyapunov Exponent |
| | |
| 4.0 | 0.10227 |
| 6.0 | 0.14037 |
| 8.0 | 0.15629 |

| C and D | |
|------------------|--------------------------|
| size of T | Lyapunov Exponent |
| | |
| 4.0 | -0.00418 |
| 6.0 | 0.05099 |
| 8.0 | 0.04740 |

CHAPTER IV

POINCARÉ SECTION ANALYSIS

Poincaré section is a graphical analysis tool used in non-linear dynamics. Poincaré section can capture interesting features such as the islands and periodic points. For example, islands are bad mixing zones. In this chapter, we will show Poincaré sections of our mixer at various flow conditions, and demonstrate destruction of islands (KAM boundaries), and increased chaotic strength.

4-1. USEFULNESS OF POINCARÉ SECTION IN CHAOTIC DYNAMICS

First of all, the concept of Poincaré section and its usefulness should be understood. Graphical methods - a hallmark of the "nonlinear dynamics" approach- tell us usually more than the analytical solution so that we use 'map' and then try to find Poincaré section. Map means casual relation between present state and next state in the future. In aspect of particle tracking, map is velocity field or velocity information. It is a deterministic rule which tells us what happens in the next time step. In Figure 4-1, let's assume that there is a plane crossed by almost all orbits in the phase space. Poincaré map is a tool developed for a visualization of the flow in the phase space of more than two dimensions. The Poincaré section has one dimension less than the phase space. The Poincaré map maps the points of the Poincaré section onto itself. It relates two consecutive intersection points. Note, that

only those intersection points counts which come from the same side of the plane [4].

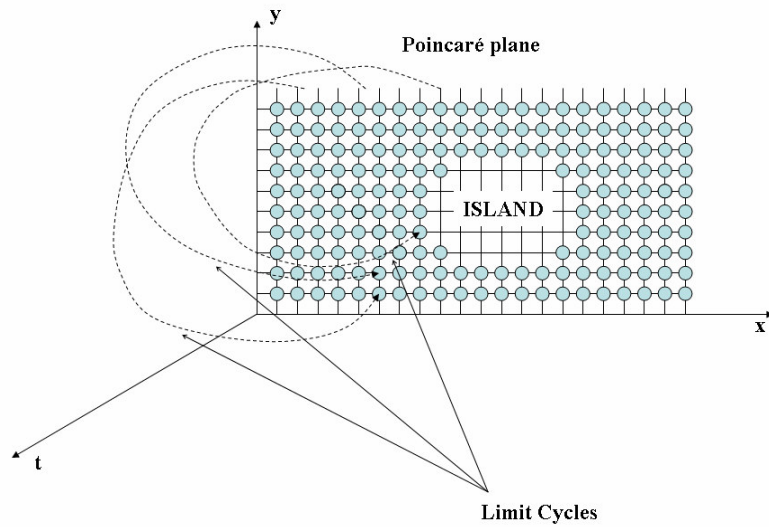


Figure 4-1. Understanding of limit cycle in three dimensional phase space

A Poincaré section is a surface in the phase space that cuts across the flow of a given system. Figure 4-2, 3 shows a Poincaré section of a three-dimensional orbit.

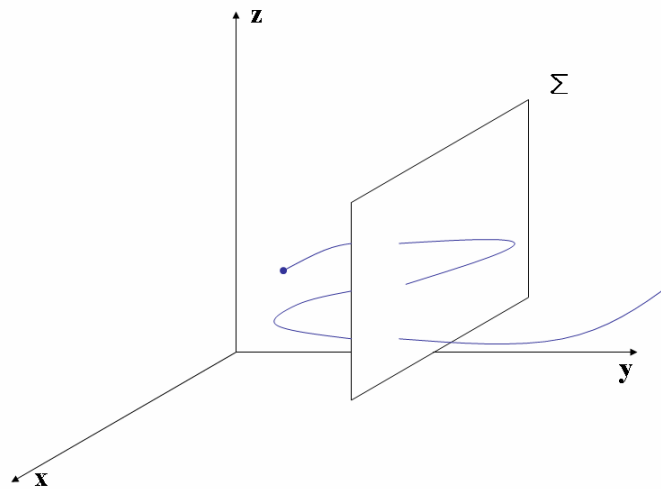


Figure 4-2. Poincaré section of a three-dimensional orbit

The Poincaré maps are useful in highlighting what solution the dynamical system is portraying through time. If for example the system is being attracted to a limit cycle, we would observe particle locations at discrete times converging to a stationary point or points, depending on the period of the solution [4].

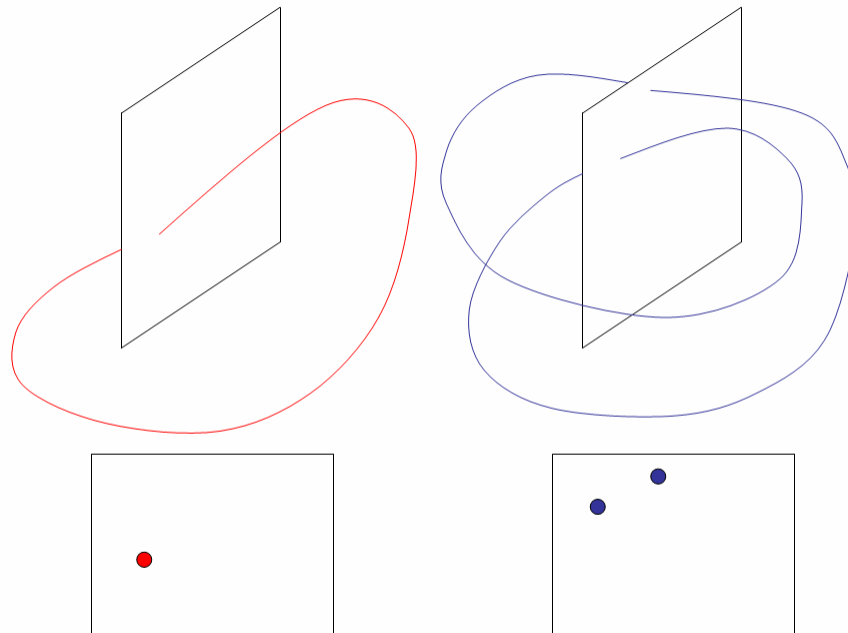


Figure 4-3. Poincaré section of periodic points. Left figure shows a single period, while right figure shows two periodic points [4]

Most nonlinear dynamics textbooks focus finding the stable state, stable point, fixed point, or to generate stable point. But in opposition, we aim to find the unstable points, since these unstable points and states are helpful to develop efficient mixers. If one can erase the stable points that make particle trajectories converge, then we can obtain efficient chaotic mixing schemes. In nonlinear dynamics, the limit cycle shows stable systems. Therefore we would like to diminish the number of limit cycles.

In two (or higher) dimensional state spaces, it is possible to have cyclic or periodic behavior. This critical behavior is represented by closed loop trajectories in the state space. A trajectory point on one of these loops continues to cycle around that loop for all the time. These loops are called cycles, and if the trajectories in the neighborhood of the cycle are

attracted towards it, we call these limit cycles. The limit cycle concept is related with the island's concept. In Figure 4-4 we show a Poincaré section, where the limit cycles form islands.

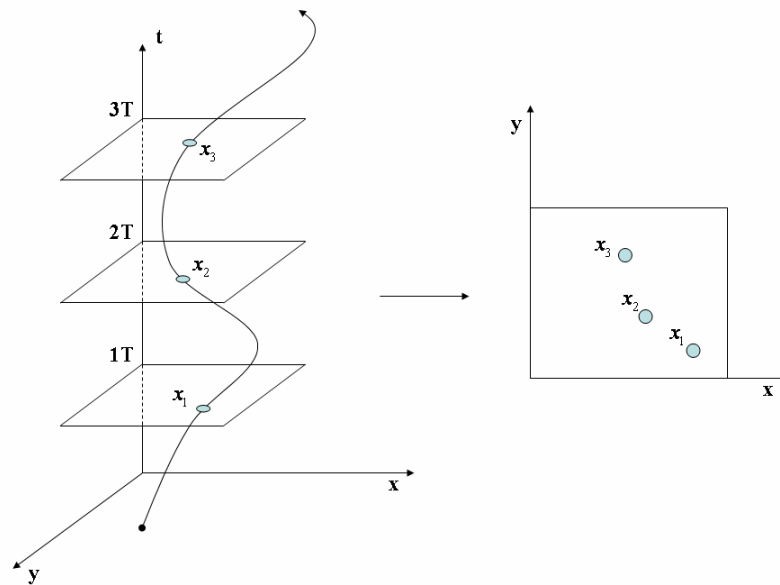


Figure 4-4. Poincaré section of 2-dimensional unsteady case [4]

4-2. POINCARÉ SECTION AND DESTRUCTION OF ISLANDS

In two dimensional cases, the passive particle's trajectory is consistent with the state space trajectory in Hamiltonian system. For this point, the stream function can be understood with nonlinear dynamics theory used in Hamiltonian system. The Eulerian velocity field derived from the stream function will represent Hamilton's equations for this system [13]. Our study is focused on how the change of period size affects the invariant manifolds and for what range of period mixing efficiency will be maximized. To study the order of particle trajectory near hyperbolic points or saddle points, a qualitative approach was used that involved the tracking of many trajectories located much closed to two neighboring saddle points.

As we know, Poincaré section is a useful tool in studying time-dependent Hamiltonian systems. It reduces the complexity of the phase space from a three-dimensional system to a two dimensional map [14]. When we change the period size, it is found that trends of periodic orbits are dependent on period size of perturbation or change of pattern. With the Poincaré-Birkhoff theorem, these periodic orbits break up into an alternating series of stable and unstable fixed points.

First of all, we tried to find best pair of pattern for most efficient mixing. In Figures 4-5 through 4-10, to form the Poincaré section, we utilized 121 markers that were uniformly distributed over the flow domain. Then we tracked these particles for 100 periods using the A-B, A-C, A-D, B-C, B-D, C-D pattern respectively, and period size was fixed as $T=6.0$. In qualitative estimation, pattern B-C case' result shows us most efficiently

dispersed state in Figure 4-8 and this result was expected when we use Lyapunov exponents in the previous chapter. Especially in A-B pattern case (Figure 4-5), one large island and small islands centered on large island are located on left top side. And in A-C case (Figure 4-6), the initial located particles can not be dispersed to left side and consequently, this empty space becomes a sort of large island. In Figure 4-7, pattern A-D case, there are four small islands in the center of phase space and empty spaces are found in left and right sides. In Figure 4-9, pattern B-D case, there are large erratic shaped island is located on left side of phase space. Finally, in Figure 4-10, pattern C-D case, in right and left side, non-negligible empty spaces still exist. With these qualitative estimations, we can decide the pattern B-C case is optimal to make best mixing case.

For detailed study, we fixed pattern case as B-C pattern case and changed the period size. If only a single flow pattern (B or C) is used, the Poincaré section would show streamlines or regular patterned particle trajectories. However, in Figure 4-11(a), 11(b), 11(c), various sized islands are shown in the Poincaré section and these islands are visible for the high frequency case $T=1.0$, $T=2.0$, $T=3.0$. And also shapes of these islands more distinct if frequency is changed to higher.

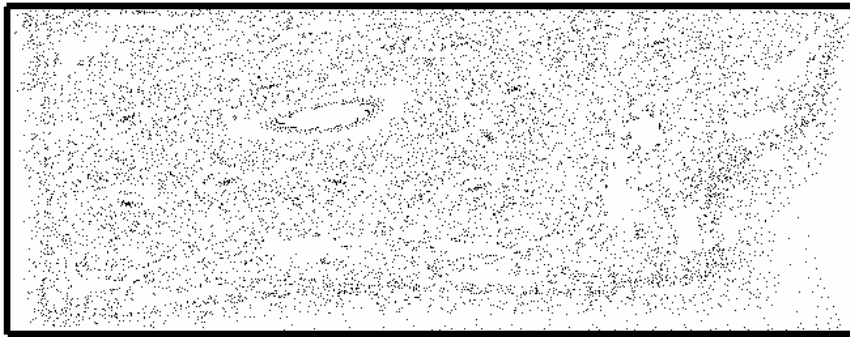


Figure 4-5. Pattern A and B ; $T=6.0$; 121 particles ; 100 periods

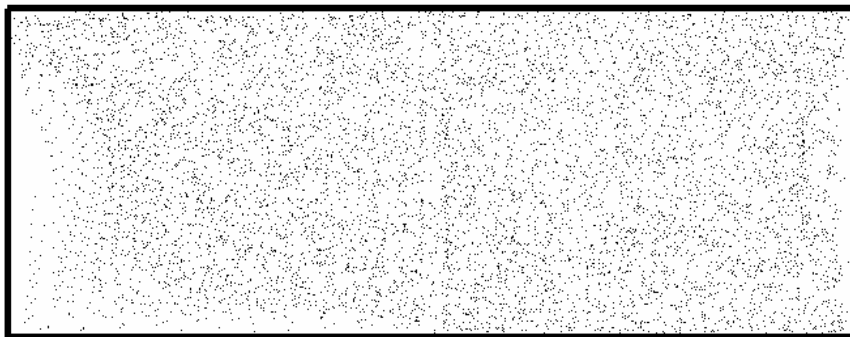


Figure 4-6. Pattern A and C ; $T=6.0$; 121 particles ; 100 periods

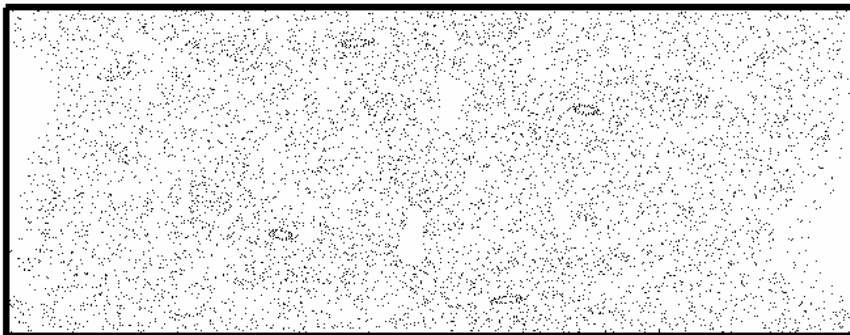


Figure 4-7. Pattern A and D ; $T=6.0$; 121 particles ; 100 periods

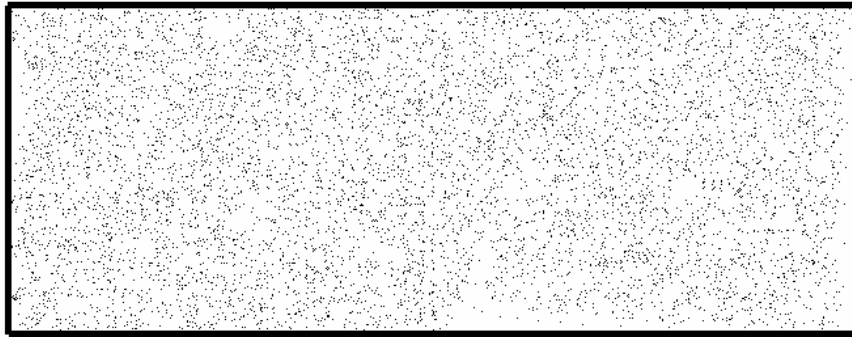


Figure 4-8. Pattern B and C ; $T=6.0$; 121 particles ; 100 periods

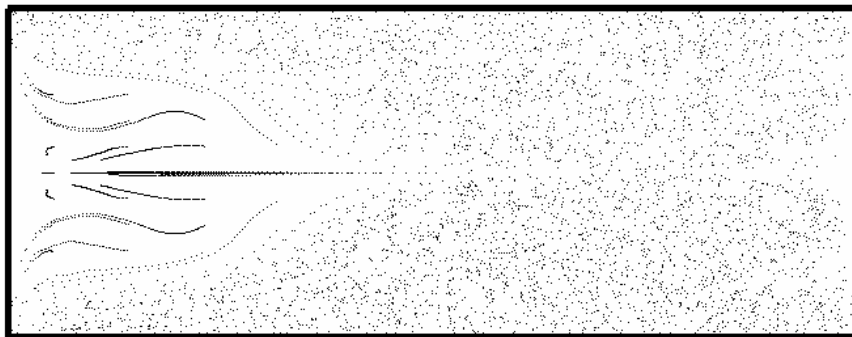


Figure 4-9. Pattern B and D ; $T=6.0$; 121 particles ; 100 periods

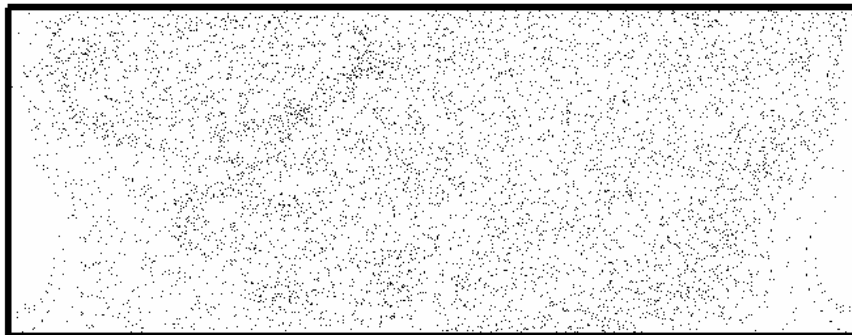
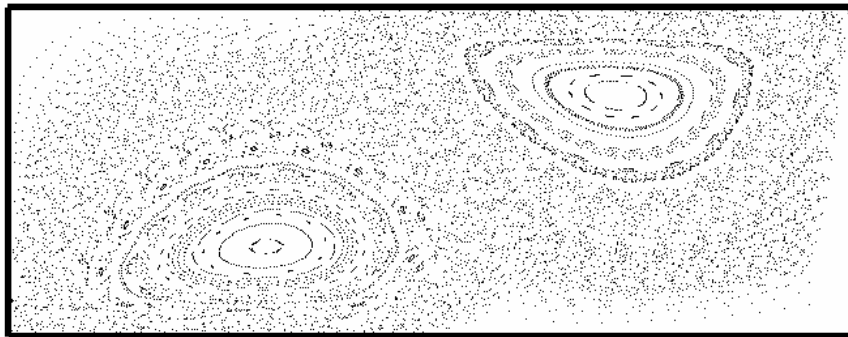
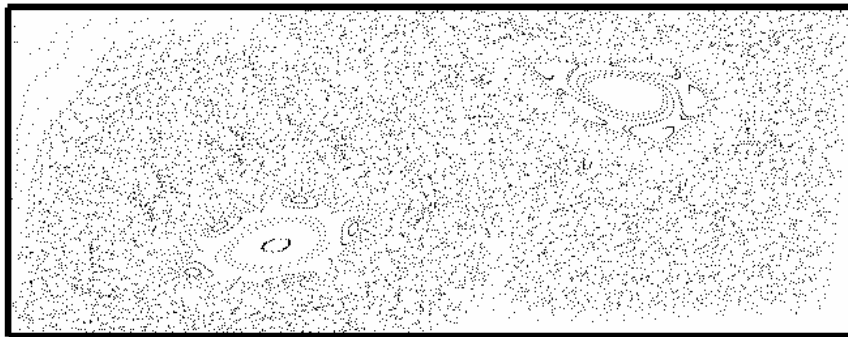


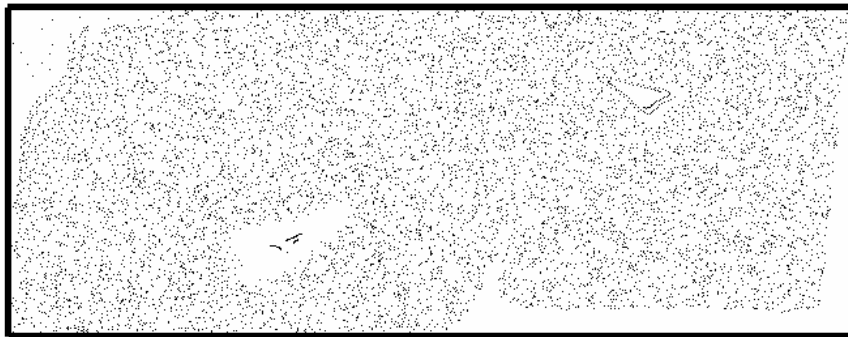
Figure 4-10. Pattern C and D ; $T=6.0$; 121 particles ; 100 periods



(a) Pattern B and C ; 121 particles ; 100 periods ; $T = 1.0$

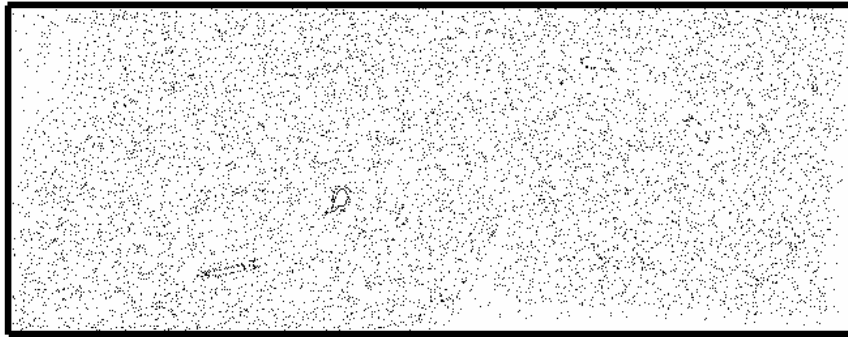


(b) Pattern B and C ; 121 particles ; 100 periods ; $T = 2.0$

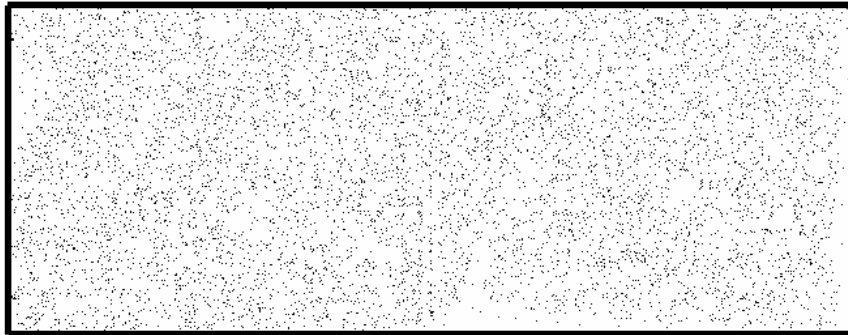


(c) Pattern B and C ; 121 particles ; 100 periods ; $T = 3.0$

Figure 4-11. Pattern B and C ; 121 particles ; 100 periods ; $T = 1.0, 2.0, 3.0, 4.0, 6.0$ We fixed pattern pair as B-C pattern and change the period size to check destruction of KAM boundaries.



(d) Pattern B and C ; 121 particles ; 100 periods ; $T = 4.0$



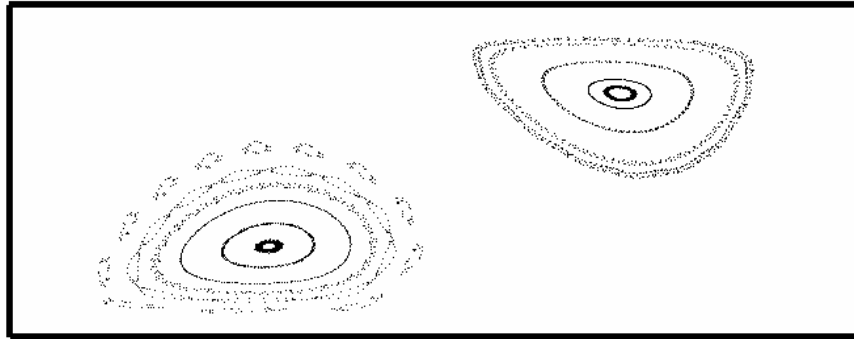
(e) Pattern B and C ; 121 particles ; 100 periods ; $T = 6.0$

Figure 4-11. continued

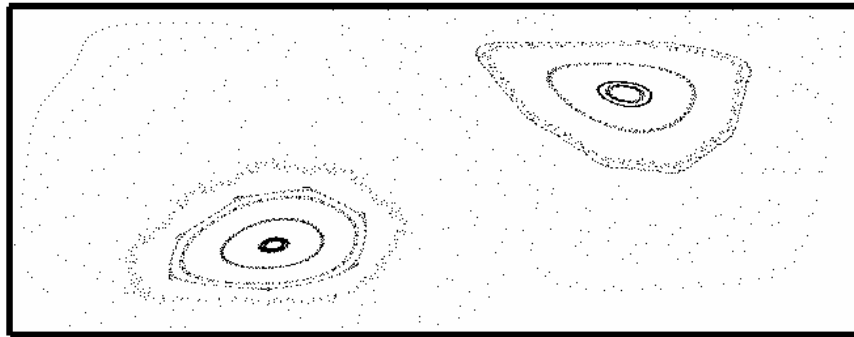
We can determine the main characteristics of chaotic mixing by the location and nature of the periodic points. Periodic points are points which return to their original position after one or more periods of flow [15,16,17]. In Figure 4-11(a), two groups of islands are located and the shapes of islands look like the solar system. By definition, in each period, particles can not penetrate the space between the small and large islands. This means that any particles that are in these islands will rotate around the islands for the rest of their motion. Therefore these islands are bad mixing zones. In Figures 4-11(e) we observe that the islands disappear with increasing the period T . We assume that removal of the islands will enable well-mixed states.

Classes of periodic points are decided according to the deformation in their nearby regions. There are elliptic stable points at the center of non-mixing rotating region and in the center of stretching, there are hyperbolic unstable points. [15, 16, 17]. Kolmogorov-Arnold-Moser (KAM) boundaries separate sea of chaos and regular territory. In other words, sea of chaos is well-mixed region or well dispersed region or territory of hyperbolic unstable points, while the regular regions are the bad-mixed zones or bad dispersed region or territory of elliptic stable points. Therefore in order to obtain chaotic mixing we should avoid the KAM boundaries as much as possible.

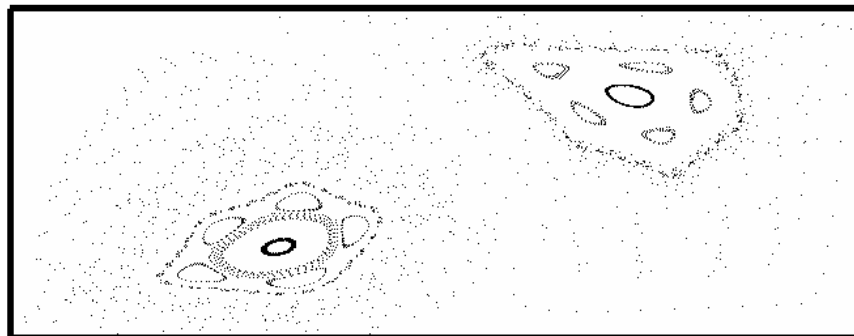
To validate our observation that increasing T destroys the KAM boundaries, we put 20 markers around the islands and regenerated the KAM boundaries by tracing particle motion for 300 time periods. Figures 4-12(a)~(f) show that the KAM boundaries are indeed destroyed by increasing the period T .



(a) Pattern B and C ; 20 particles ; 300 periods ; $T = 1.0$

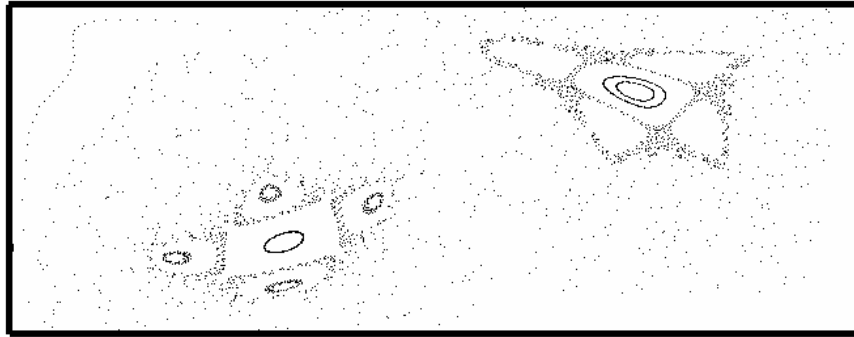


(b) Pattern B and C ; 20 particles ; 300 periods ; $T = 1.5$

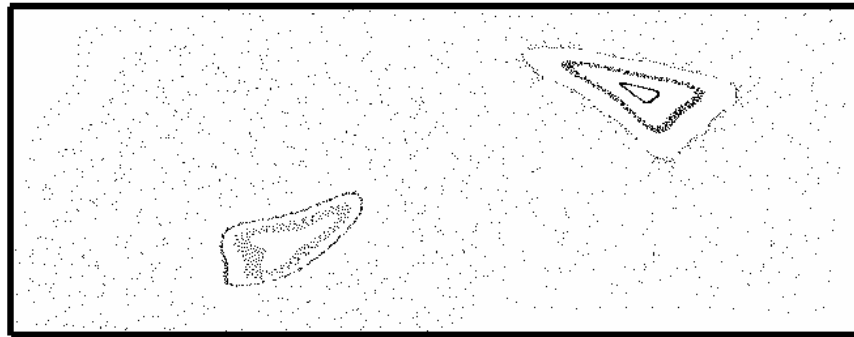


(c) Pattern B and C ; 20 particles ; 300 periods ; $T = 2.0$

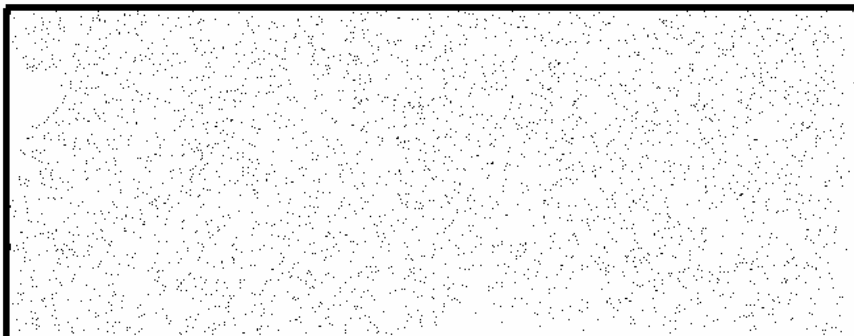
Figure 4-12. Pattern B and C ; 20 particles ; 300 periods ; $T = 1.0, 1.5, 2.0, 2.5, 3.0, 6.0$



(d) Pattern B and C ; 20 particles ; 300 periods ; $T = 2.5$



(e) Pattern B and C ; 20 particles ; 300 periods ; $T = 3.0$



(f) Pattern B and C ; 20 particles ; 300 periods ; $T = 6.0$

Figure 4-12. continued

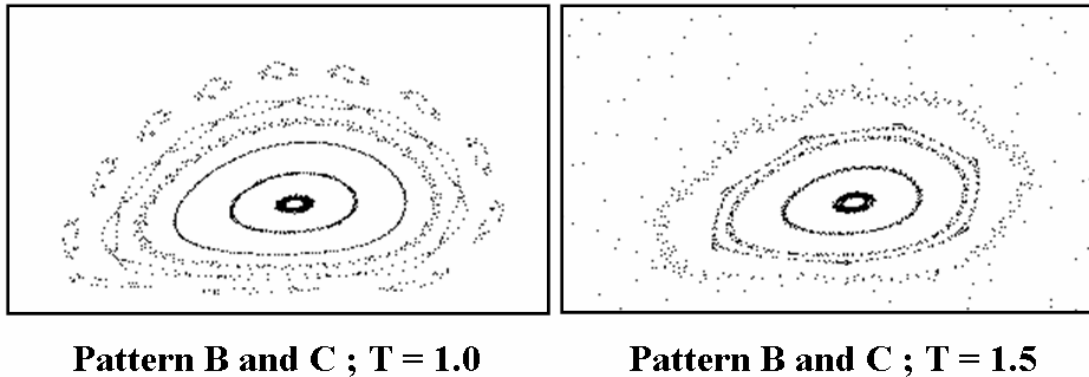


Figure 4-13. Islands @ Pattern B and C ; T = 1.0, 1.5

In Figure 4-13, the process of breaking up of the KAM curves and area separating starts from T=1.5 case. We can find that some regular areas change to chaotic areas with the breaking up of the outer KAM curves. In high frequency case, the perturbation doesn't destroy all the features of the unperturbed phase space, because KAM (Kolmogorov-Arnold-Moser theorem) boundaries prevent the effects of perturbation. In other words, KAM boundaries on the inside and outside limit the stochasticity that occurs around the hyperbolic points. This prevents the stochastic trajectories from wandering through other parts of phase space [14, 18].

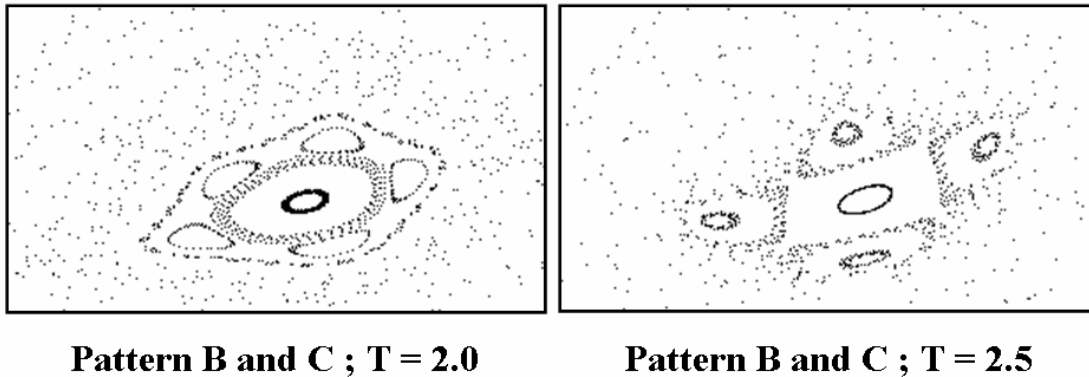


Figure 4-14. Islands @ Pattern B and C ; T = 2.0, 2.5

This means that islands can be removed as chaotic strength increases. In Figure 4-14, five small islands in case of $T=2.0$ are destroyed in case of $T=2.5$. These island chains obviously tend to limit the stochasticity of trajectories by preventing them from wandering to other areas of phase space. On the other hand, the pronounced gaps that exist in the cantori structures allow stochastic trajectories to reach a wider ranging area of phase space [14, 18]. Finally, in Figure 4-15, the islands are destroyed and this area becomes chaotic. This fact shows that increased chaotic strength causes destruction of the KAM boundaries, as stated by the KAM theorem [17].

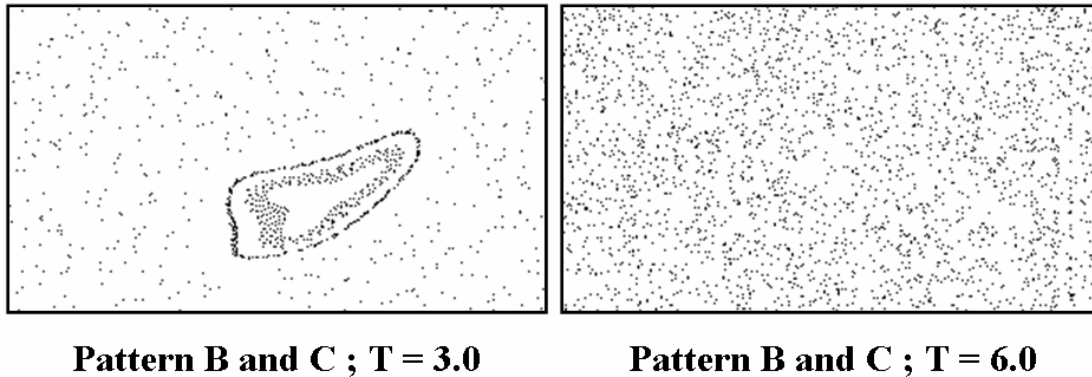


Figure 4-15. Islands @ Pattern B and C ; $T = 3.0, 6.0$

Before breaking up, although particles in these inner chaotic areas move in a chaotic regime, the stretching and folding are confined to a very limited area, and good mixing cannot be achieved in these areas because most of these inner chaotic areas lie on one side of the interface line. These inner chaotic areas also include some periodic areas. This kind of nesting of multiple layers is a prominent character of nonintegrable Hamiltonian systems [10].

In Figure 4-11, we present the Poincaré sections obtained for pattern B-C at periods $T=1, 2, 4$, and 6 . The Poincaré sections are obtained by tracking the motion of 121 particles for 100 time periods. Islands of bad mixing zones are observed for $T=1, 2$ cases. The island boundaries, also known as the Kolmogorov-Arnold-Moser (KAM) boundaries, separate the chaotic and regular regions of the flow [17]. In the figure, we also present the KAM boundaries, obtained by tracking 20 particles that were initially located on the KAM boundaries, for 300 periods. We observe reduction in the bad mixing zone with increased T . For example, the islands disappear for $T \geq 6$. The Poincaré section for $T=8$ is qualitatively

similar to that of the $T=6$ case, and it not shown in the figure. Destruction KAM boundaries is desired for enhanced mixing, but is not the sufficient condition for the best mixing case. For example, the FTLE for $T=6$ is considerably larger than that of the $T=8$ case, and it corresponds to the best mixing case among the flow patterns and frequency ranges studied in (Kim, 2004). We must indicate that the FTLE values presented above were obtained for particles that were outside the bad mixing zones.

CHAPTER V

STRETCHING OF INTERFACE

Behavior of interface between two liquids has an important role in mixing case. In chaotic mixing state, exponential growth of interface shows how efficiently particles are dispersed. Stretching and folding are key issues in chaotic mixing and calculation of stretching rate relates with measurement of dispersing degree directly. In this chapter, we will show exponential growth of stretching of interface and then explain relation between stretching of interface and Lyapunov exponent.

5.1 DEFINITION OF STRETCHING OF INTERFACE

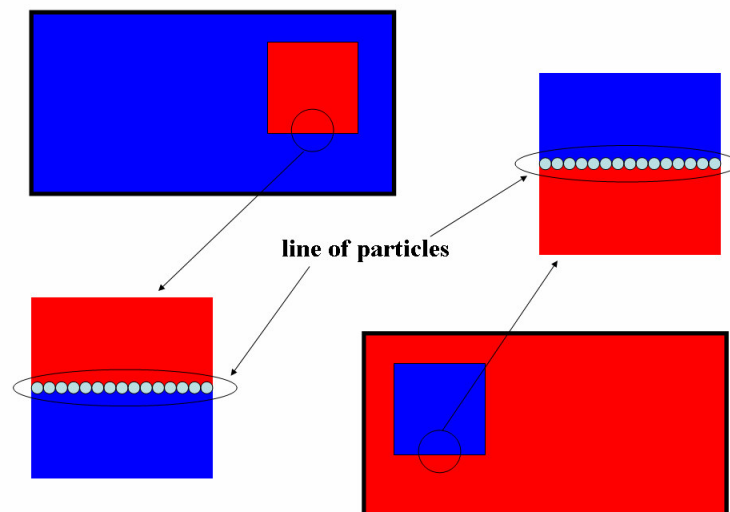
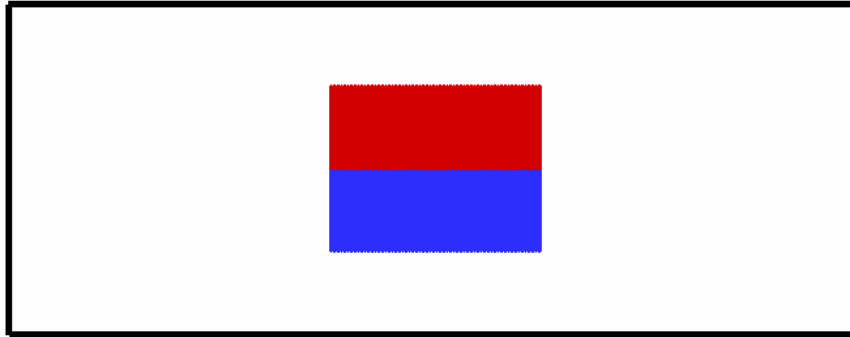
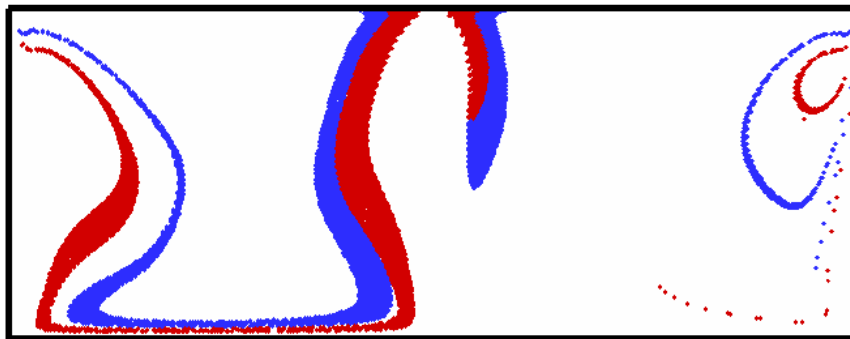


Figure 5-1. Line of particles

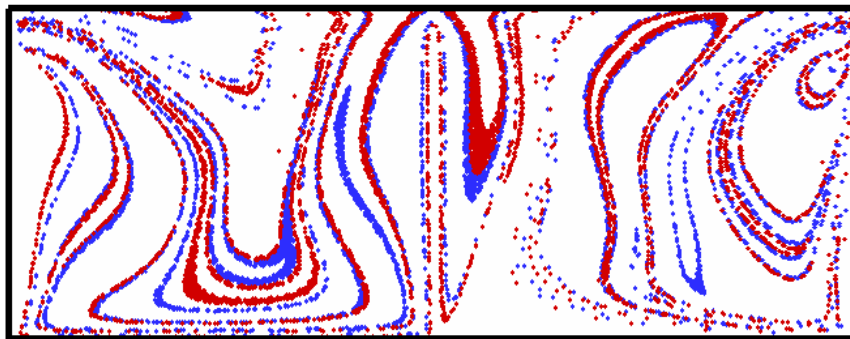
To quantify the degree of mixing, we consider the stretching of a line of particles.



(a) Initial interface between red blob and blue blob

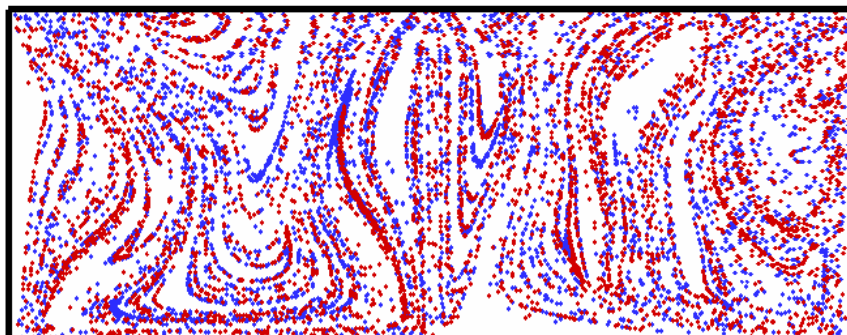


(b) interface stretching between red blob and blue blob at 2 periods

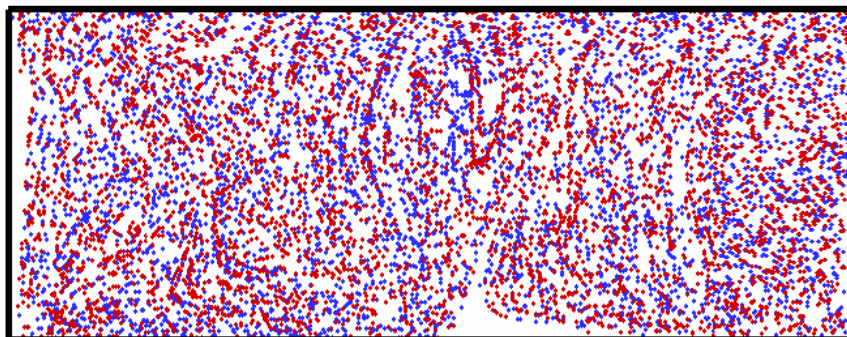


(c) interface stretching between red blob and blue blob at 4 periods

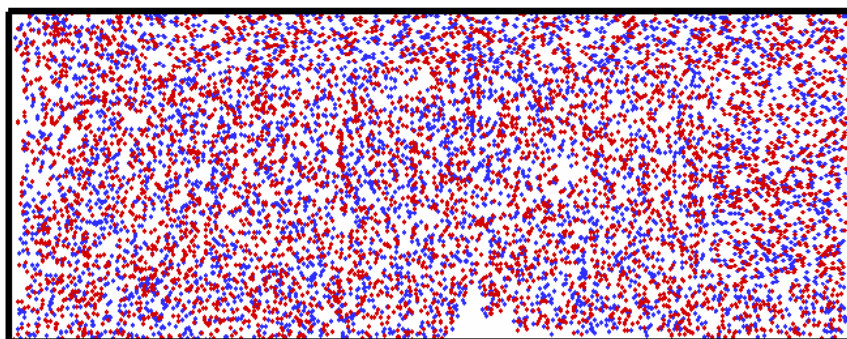
Figure 5-2. Interface stretching evolution : B and C pattern $T=6.0$ case, with 10000 particles



(d) interface stretching between red blob and blue blob at 6 periods



(e) interface stretching between red blob and blue blob at 8 periods



(f) interface stretching between red blob and blue blob at 10 periods

Figure 5-2. continued

If $S(0)$ is summation of an infinitesimal distance between adjacent two particles on a line of particles for the initial condition as shown in Figure 5-1, $S(t)$ is the corresponding change at nondimensional time τ , the line stretching is

$$\lambda = \frac{S(\tau)}{S(0)} \text{ or } \ln \lambda = \ln \left(\frac{S(\tau)}{S(0)} \right). \quad (5.1)$$

As we see in Figure 5-2, the line stretching exhibits a great exponential growth [17, 19, 20, 21, 22]. Ottino [17] stated that the line stretching has trend of exponential growth,

$$S(\tau)/S(0) = \exp(\text{Lyapunov Exponent} \cdot \tau).$$

So we can find relationship between line stretching and Lyapunov exponent. To decide optimum frequency, Lyapunov exponents had been calculated for various cases in previous chapter.

First, we calculated stretching of line consisted with 100 particles and initial length $S(0)$ is 0.2. The reason why initial length is short is to get enough precision and we were sure that this short line will grow exponentially because mixing system is chaotic state. As we know B and C pattern with $T=6.0$ case is most chaotic, the growth rate of this case is fastest and exponential. In Figure 5-3, growth of line stretching of B and C pattern at $T=6.0$ case is most exponential and fastest. To verify trend of exponential growth, we made log-linear graph for B and C Pattern at $T=4.0$ and $T=6.0$ cases. In Figure 5-4, we can check exponential growth of two cases.

But, in Figure 5-5, after about non-dimensional time 40, growth of line stretching is saturated. This is natural result because our mixing zone is a closed space. In Figure 5-6,

there is exponential growth of stretching ratio with 1000 particles and in Figure 5-7, although the number of particles is different for each case, order of growth of stretching ratio is similar.

If mixing zone is open space, line stretching will grow infinitely with exponential aspect. Nishimura et al. made similar results about line stretching in quasi-periodic cavity case and they concluded that saturation point is a matter of course in closed space. Also they found saturation point will be independent if number of particle is enough, for example, above 3000 [21]. In linear-linear graph-Figure 5-8(a), maximum saturation value is just 700 because number of particles is only 100. But, in Figure 5-8(b), when 1000 particles are used, the maximum saturation value is 7000. This saturation value will be converged if above 3000 particles are used.

In this time, the reason why value of stretching rate is saturated is explained using graphical result. In Figure 5-9, there are snap shots of corresponding changes of line at non-dimensional time. In right side, there are connection lines between two adjacent particles. After non-dimensional time 20.0, destruction of structure begins. In snap shot of non-dimensional time 40, particles set up line are totally dispersed. Because particles are dispersed in closed space and their positions have limited within finite mixing zone, with definition of line stretching value, stretching rate is saturated after enough time. And as we see Figure 5-2(e) and 5-2(f), dispersing state is similar with previous state if particles are dispersed totally. So we can conclude that stretching rate of closed mixing zone is saturated after enough time.

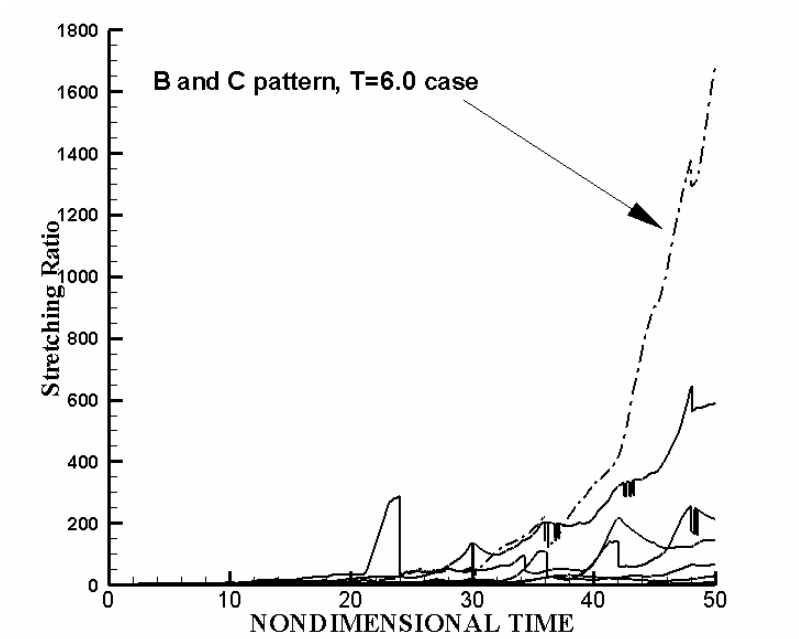


Figure 5-3. Interface stretching with 100 particles for various cases

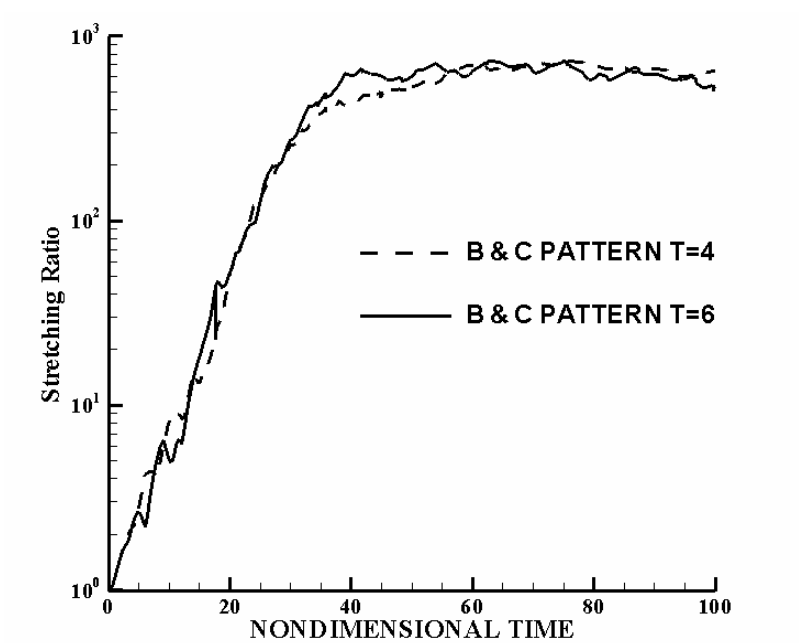


Figure 5-4. Comparison between B and C pattern T=4.0 case and T=6.0 case (100 particles case).

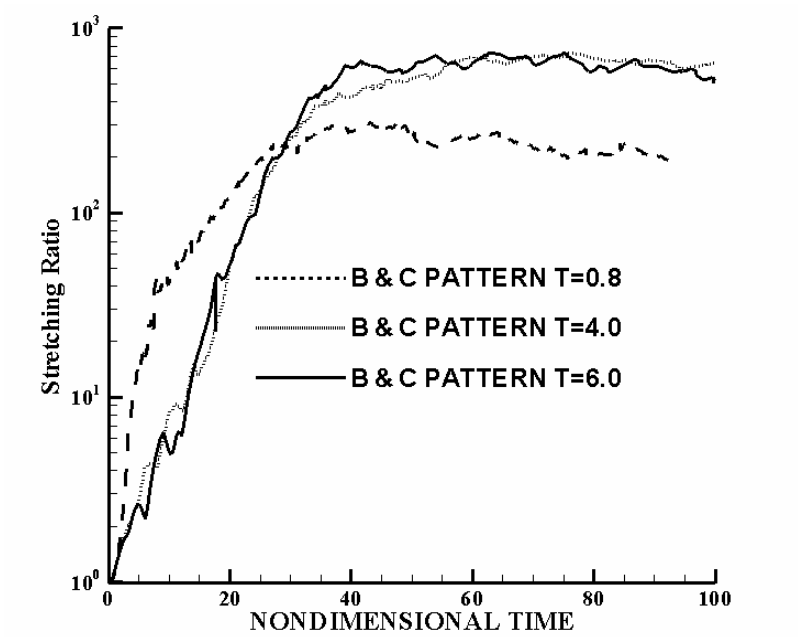


Figure 5-5. Stretching values are saturated after 50 non-dimensional time because mixing zone is closed space (100 particles case).

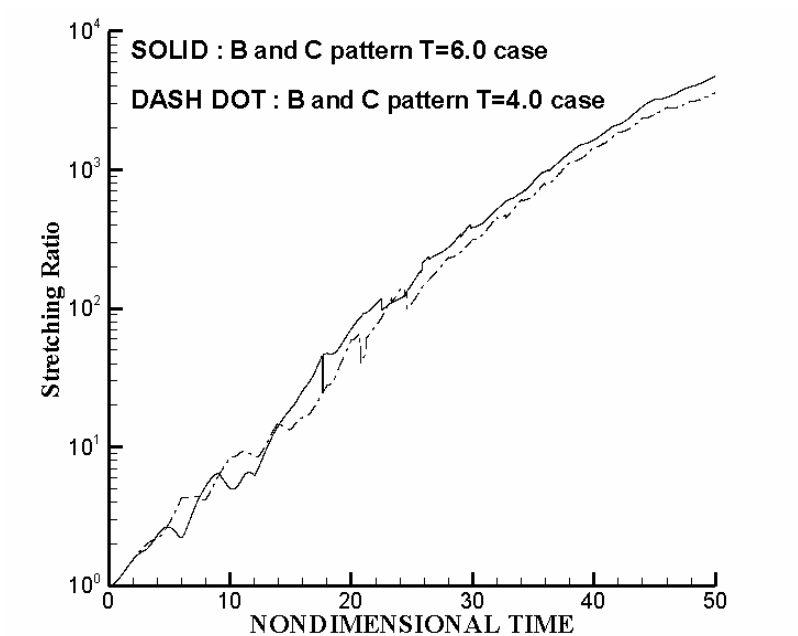
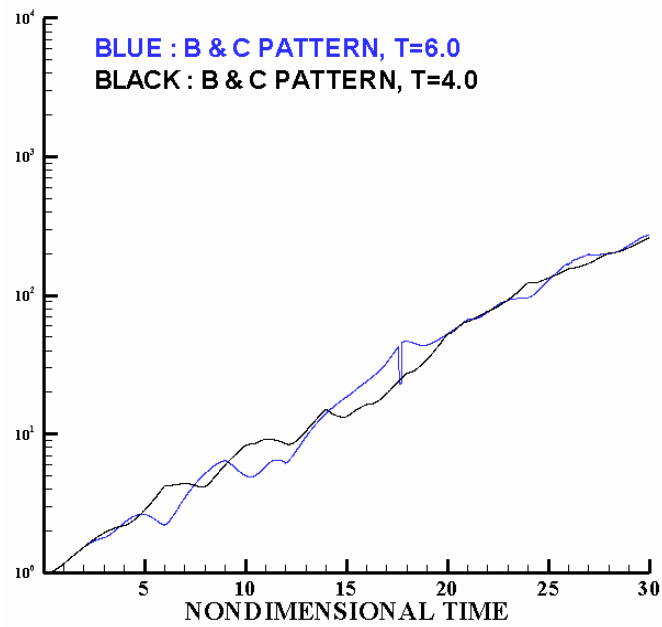
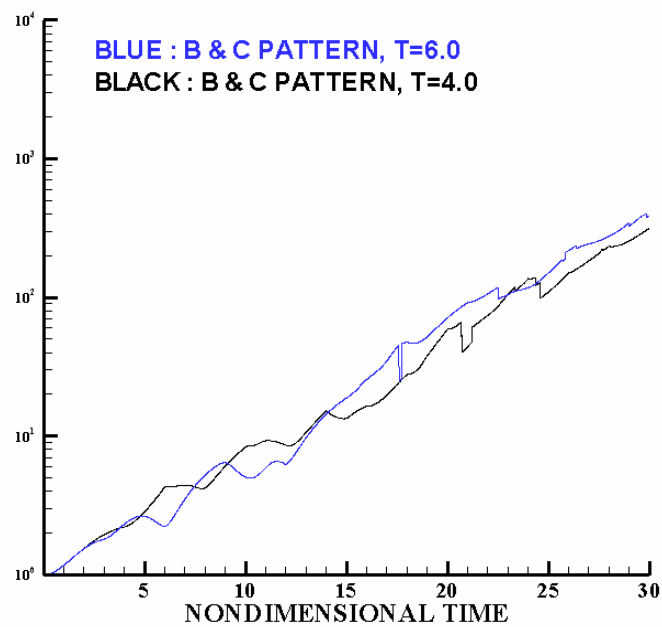


Figure 5-6. Exponential growth of stretching ratio with 1000 particles

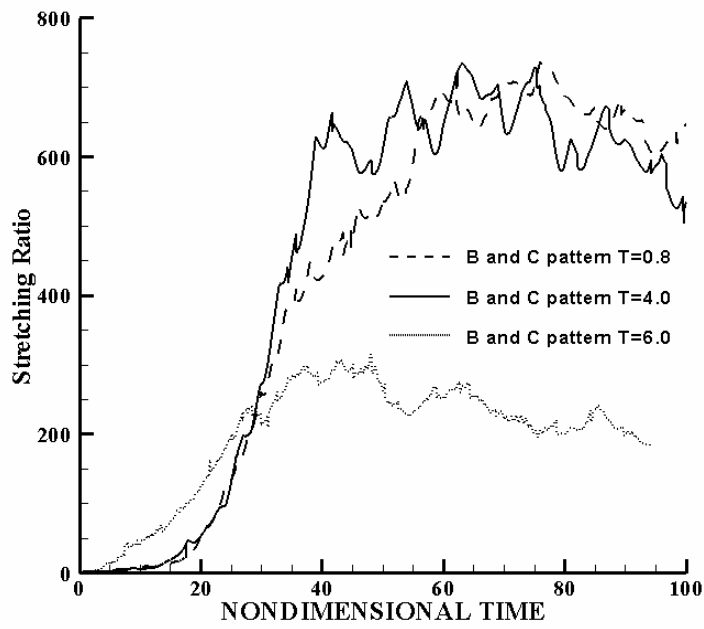


(a) number of particles = 100

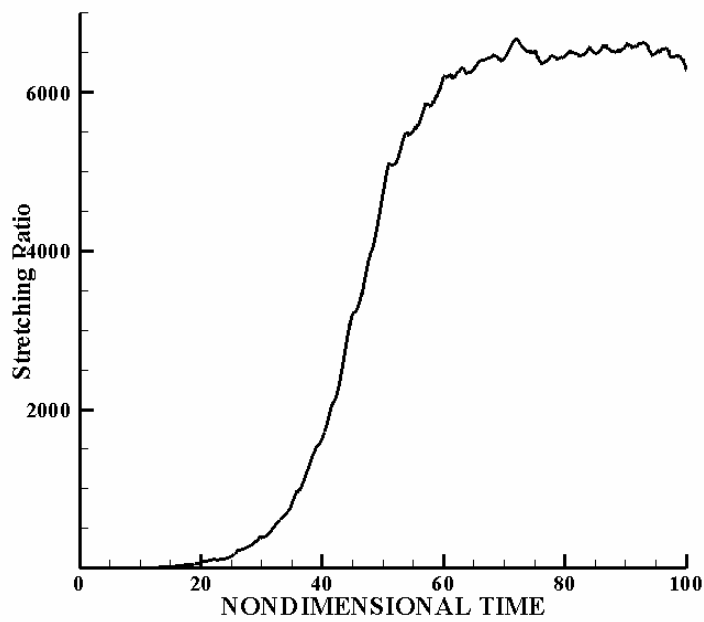


(b) number of particles = 1000

Figure 5-7. Exponential growth of stretching ratio with (a) 100, (b) 1000 particles. Although the number of particles is different for each case, order of growth of stretching ratio is similar.



(a) linear - linear scale (100 particles)



(b) linear - linear scale (1000 particles)

Figure 5-8. Different saturation points - B and C pattern (100, 1000 particles)

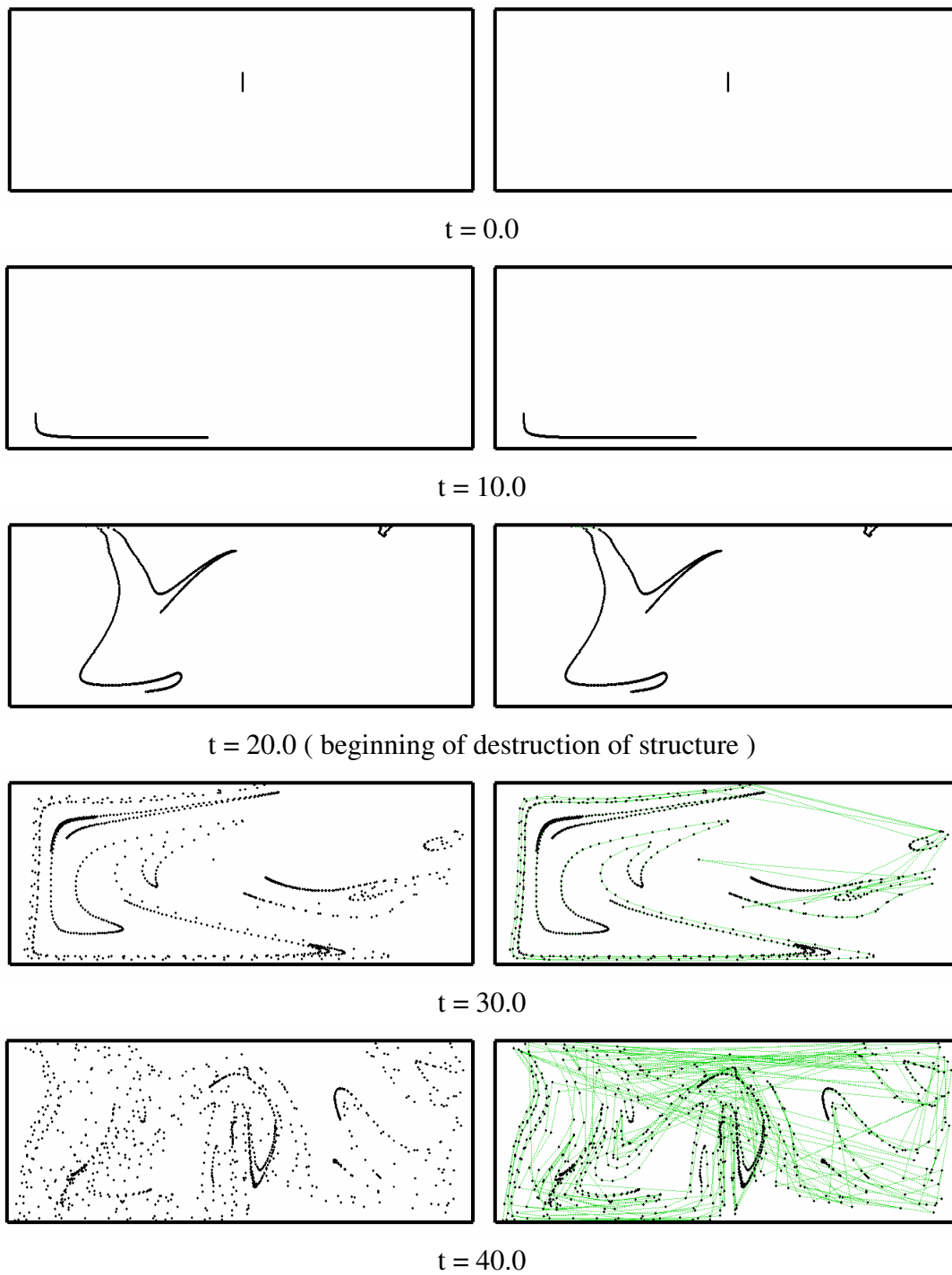


Figure 5-9. Snap shots of stretching of interface (B and C pattern , size of $T = 4.0$, 1000 particles)

5.2 STRETCHING RATE AND LYAPUNOV EXPONENT

As we stated in previous sub chapter, the line stretching in chaotic system exhibits a great exponential growth and this exponential growth gives us an important hint to find useful characteristics of chaotic system [22]. Ottino [17] stated that the line stretching has trend of exponential growth,

$$S(\tau)/S(0) = \exp(\text{Lyapunov Exponent} \cdot \tau). \quad (5.2)$$

In Figure 5-10, we calculated stretching exponent in B and C pattern at T=6.0 case with 100, 1000, 3000 particles. As we expected, with increasing of number of particles, stretching exponent is increased. This means that the finally converged exponent indicates Lyapunov exponent with same value if enough precision is satisfied.

As Ottino expected [17], we find converged Lyapunov exponent is same with stretching exponent. This means we verify that above equation is reasonable. In Figure 5-11, stretching exponent is converged to about 0.3 and Lyapunov exponent of B and C pattern at T=6.0 case is about 0.3 in Figure 5-12. And in Figure 5-11 and 5-12, the trend of stretching rate corresponds to the order of Lyapunov exponent[23, 24]. In next chapter, we will explain about particle dispersing and the trend of particle dispersing also corresponds to the trend of Lyapunov exponent and stretching rate.

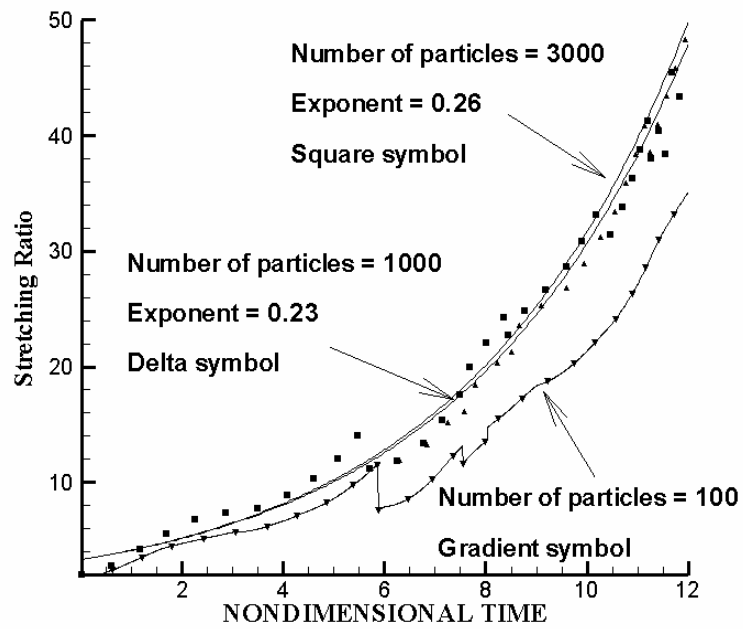


Figure 5-10. Exponential growth of interface stretching : With increasing number of particles, the stretching exponent increases

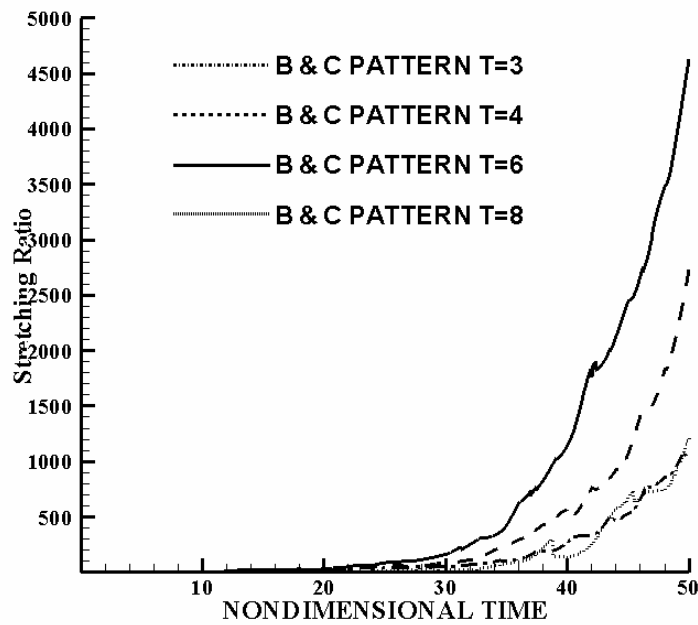


Figure 5-11. Exponential growth of interface stretching with 100 particles: this graph shows relation between Lyapunov exponent and stretching exponent

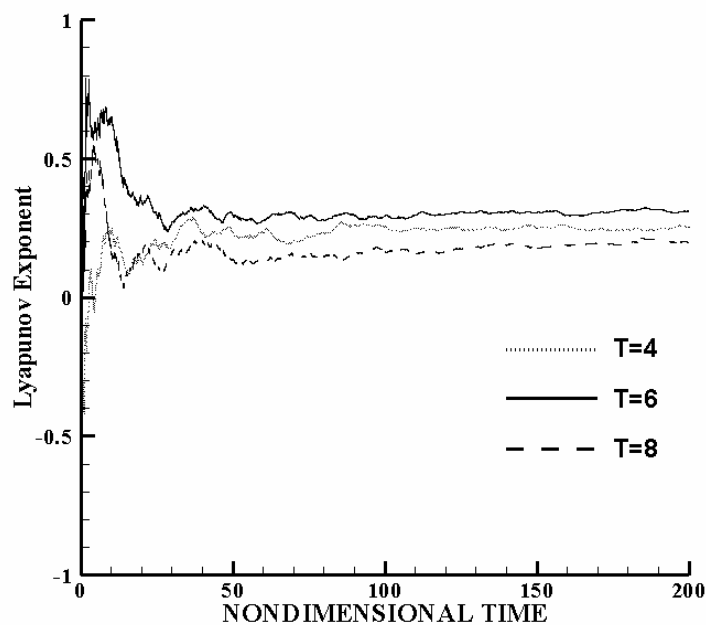


Figure 5-12. We can find relation between converged Lyapunov exponent and converged value of stretching

5.3 LINE STRETCHING AND HYPERBOLIC FIXED POINTS

In previous work, we found critical weak points in measurement method of stretching field. Due to destruction of structure, the snap shots of stretching field cannot have physical meaning any more. The reasons are explained below.

- Initial length was too long and also initial precision was not enough due to small number of particles.
- Our measurement has only local meaning.
- With superposition, although we can look for fixed points and Lyapunov exponent, we lost useful information.

With above reasons, we changed the basic idea to measure length of interface or stretching ratio. The new idea is very simple. Instead of one initial line, we split line into small fragments. These fragments are fluid elements. Our goal is focused on very thin structure (line) so that these fragments have enough roles. In Figure 5-13, there are five fragments' snap shots. As we stated before, the order of stretching ratio follows the order of Lyapunov exponent in Figure 5-14. Using fragments, local stretching can be considered and also, we can check the positions of hyperbolic fixed points-crossing points of line elements using Poincaré section in Figure 5-15.

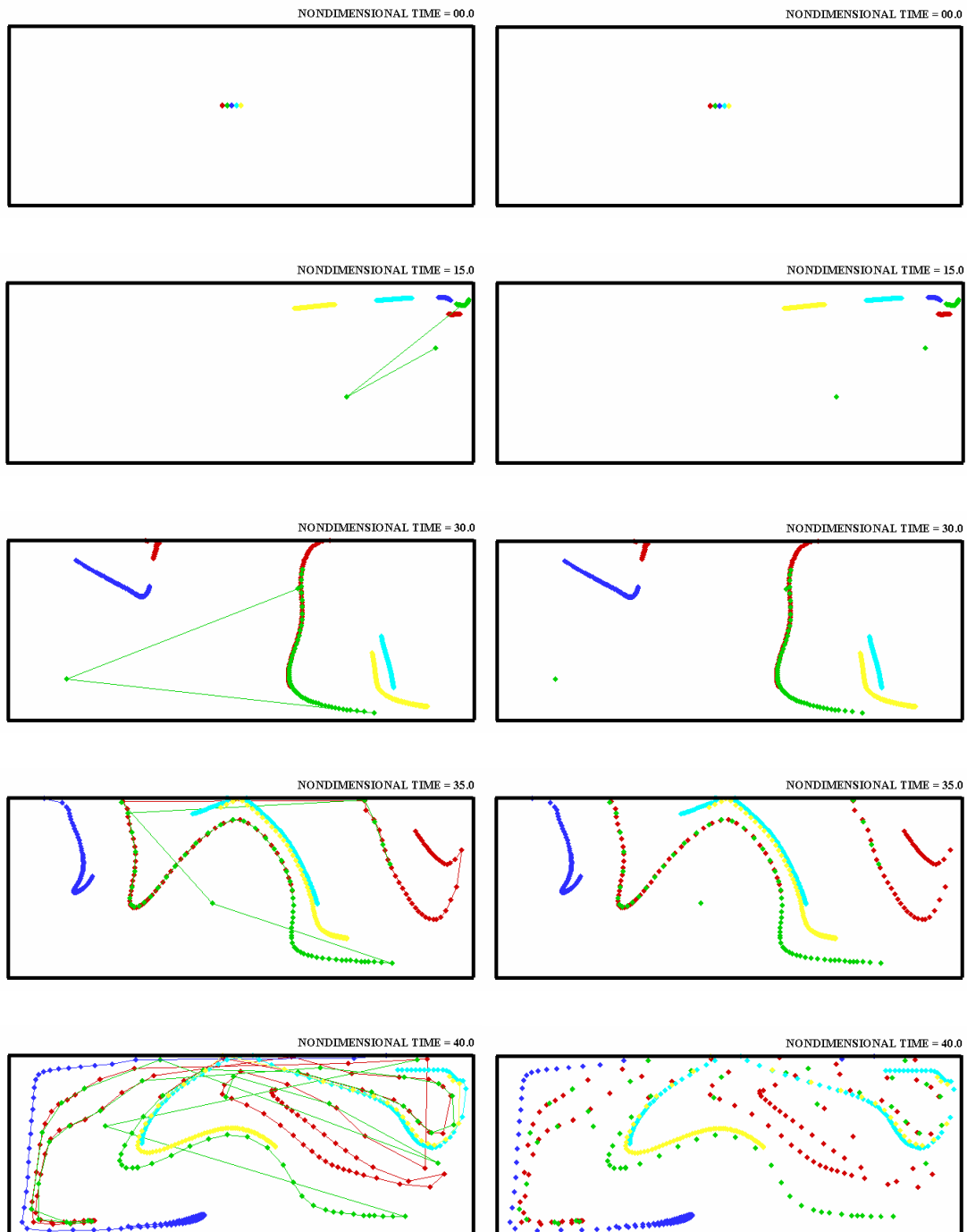


Figure 5-13. Snap shots of stretching of interface
(B and C pattern , size of $T = 6.0$, 500 particles)

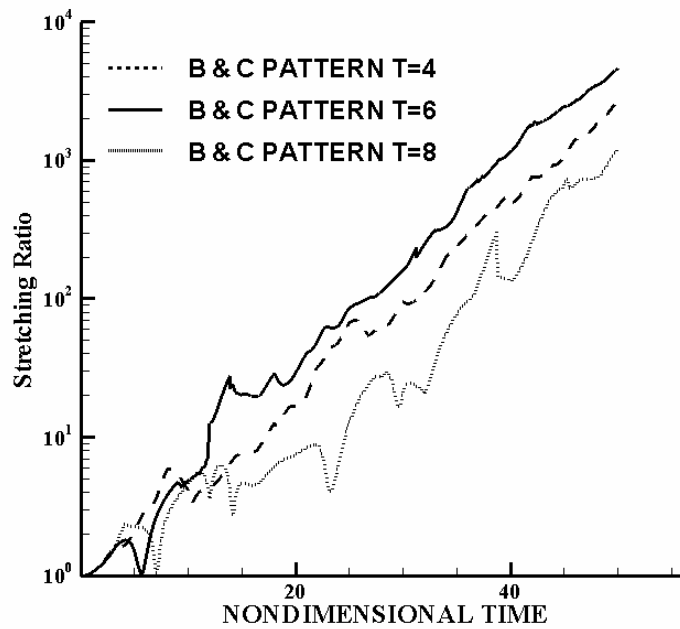


Figure 5-14. Stretching ratio : The order of stretching ratio follows the order of Lyapunov exponent.

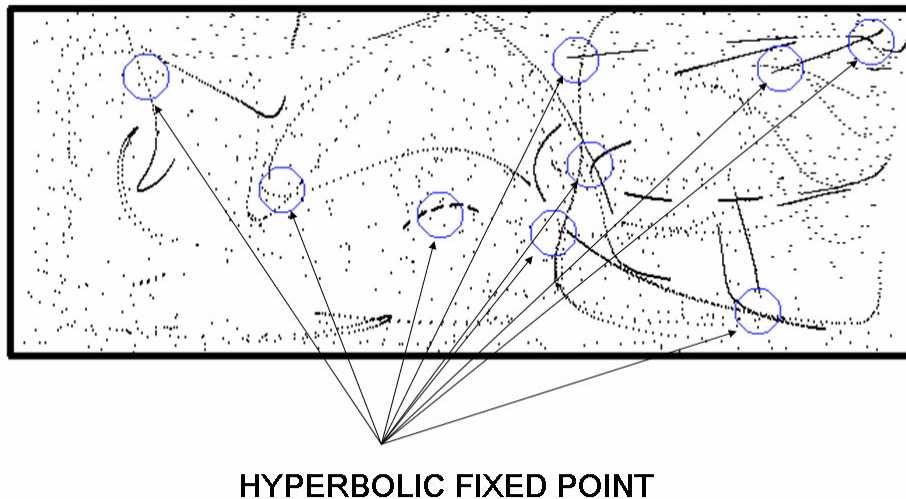


Figure 5-15. Positions of hyperbolic fixed points

CHAPTER VI

PARTICLE SPREAD

In this chapter, we present box counting method to measure mixing index intuitively. If the snapshots of mixing simulation are given, it maybe is easy to estimate mixing state. In our case, if particles are dispersed uniformly through whole mixing zone, this state can be considered as well-mixed state. But this measurement is just qualitative method. For quantitative measurement, reasonable method to decide mixing state is required. Box counting method is easy way and also intuitive, direct, reasonable. With these reasons, we tried to calculate mixing index using box-counting method.

6.1 DEFINITION OF BOX COUNTING METHOD

The box counting calculation method quantifies the rate at which particles are dispersed by the flow into small uniform boxes [25]. Selecting appropriate size of box is important. If the boxes are too large, the method will quantify mixing only on a coarse scale. On the other hand, if the cells are too small, only a small portion of the boxes will be occupied at any given time. Several criteria can be adopted to select the box size. Jones[26] recognized that a perfectly randomized population of particles has a Poisson bin-occupancy distribution, and used this information to determine a box size so that on average there was one particle per cell. The final goal of this approach is to find homogenization of particle

spread state through whole mixing domain. We divide the mixing domain into K boxes, area of each box is a . The total area is same with area of mixing zone. So, the equation is $Ka=A=mixing\ zone$. For M particles, the particle density is $\rho=M/K$. We define homogenization as the condition that the probability a particle is in a given bin is

$$a/A.$$

First of all, we suppose that all boxes are equiprobable. Next we wish to determine the distribution of boxes containing exactly m particles, assuming this condition is satisfied [26]. This is a sort of typical occupancy problem that is well established in probability theory. It is easy to show that the solution is the Poisson distribution

$$q_{\rho}(m) = (\rho^m / m!) e^{-\rho}. \quad (6.1)$$

The number of boxes containing m particles is

$$Kq_{\rho}.$$

The mean number of particles per box is, of course, ρ . In our case, this box size is chosen so that for a perfectly random distribution of particles, 98% of the boxes contain at least one particle. Numerical tests indicate that such a box size is approximately given by

$$s \sim 2N^{\frac{1}{2}}, \quad (6.2)$$

where s is the size of the box and N is the total number of particles. If the simulation is made with 10,000 particles, appropriate box size is decided as $s=0.02$.

6.2 HOW TO CALCULATE MIXING INDEX

Let's assume there are 40,000 particles are dispersed in 10,000 cells. In ideal mixing state, there should be 4 particles in each cell to make well mixed state as below

$$\rightarrow \frac{40,000 \text{ particles}}{10,000 \text{ cells}} = 4.0 \text{ particles / cell}$$

But, in real case, the number of particles contained in each cell can be various.

I. 0 particle \rightarrow bad mixed state

II. 1~3 particles \rightarrow regular mixed state

III. 4 particles \rightarrow well mixed state

IV. 5+ \rightarrow bad or regular mixed state

In case IV, the number of particles should be counted down to 4. This is important point for homogeneity. And then, for each cell, calculate the rate of number of particles. We call the rate of number of particle as 'box rate number'.

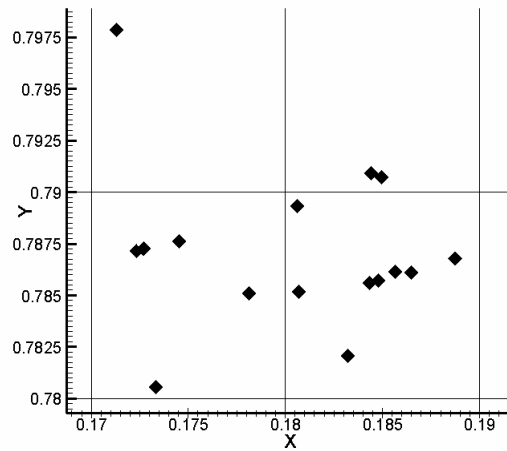


Figure 6-1. Particles located in cells

If we calculate box rate number for Figure 6-1 case,

$$\text{box rate number} = \frac{5.0}{4.0} \rightarrow \frac{4.0}{4.0} (\text{discounted}) = 1.0$$

$$\text{box rate number} = \frac{8.0}{4.0} \rightarrow \frac{4.0}{4.0} (\text{discounted}) = 1.0$$

$$\text{box rate number} = \frac{2.0}{4.0} \rightarrow \frac{2.0}{4.0} = 0.5$$

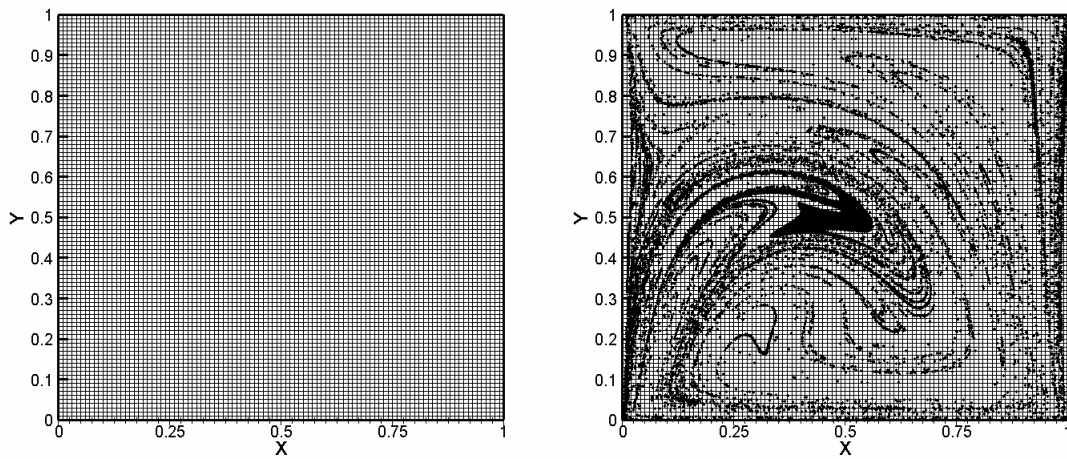
$$\text{box rate number} = \frac{1.0}{4.0} \rightarrow \frac{1.0}{4.0} = 0.25$$

After calculating the box rate number for all boxes, make the average number of all box rate number. This average value will be “Mixing Index”.

If we consider only 4 boxes in Figure 6-1,

$$\text{Mixing Index} = \frac{1.0 + 1.0 + 0.5 + 0.25}{4} = 0.6875$$

To apply to real case, we referred to Ling et al's share case [9]. They used discontinuous cavity flow caused by alternating motion of the top and bottom walls of a rectangular cavity. This model is very simple to generate and also practical and efficient. In Figure 6-2, there are example of 40,000 particles calculation case and we can compare the precision difference with change of box size in Figure 6-3.



100X100 boxes

Figure 6-2. Size of cell for 40,000 particles case

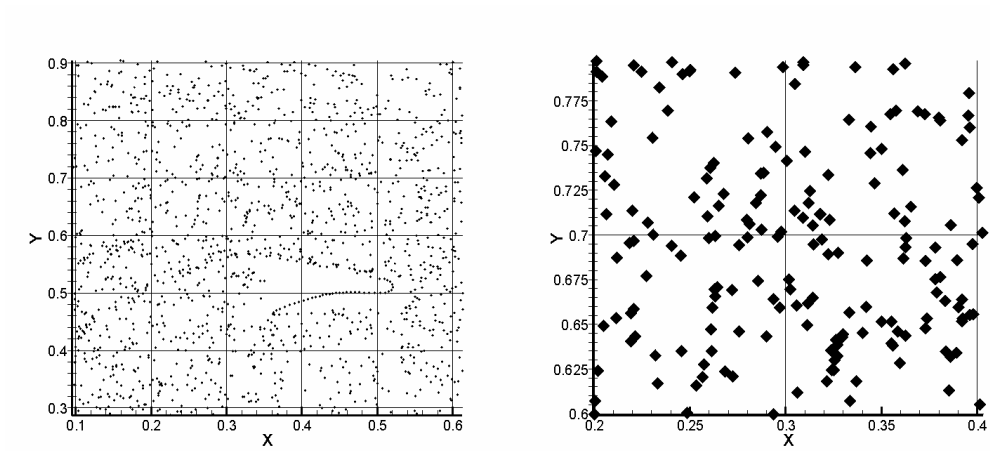


Figure 6-3. Coarse selection of box size

In Figure 6-4, 5, 6, there are cases of evolution of deformation of blob. In each case, we changed the size of T , as we expected, mixing index grows differently. In Figure 6-7, we summarized mixing indices for each case.

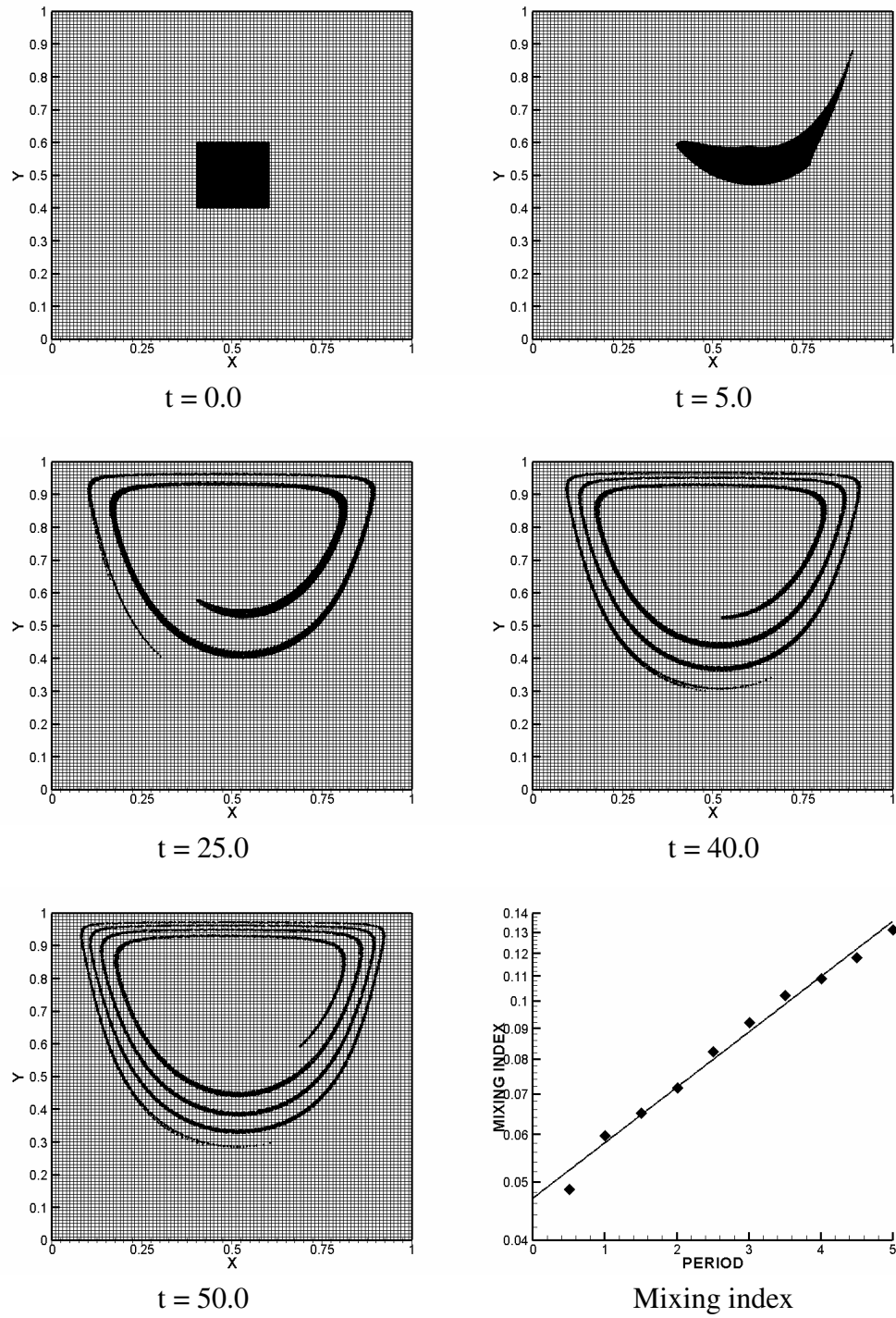


Figure 6-4. Steady case , 10000 particles ; $T=10.0$

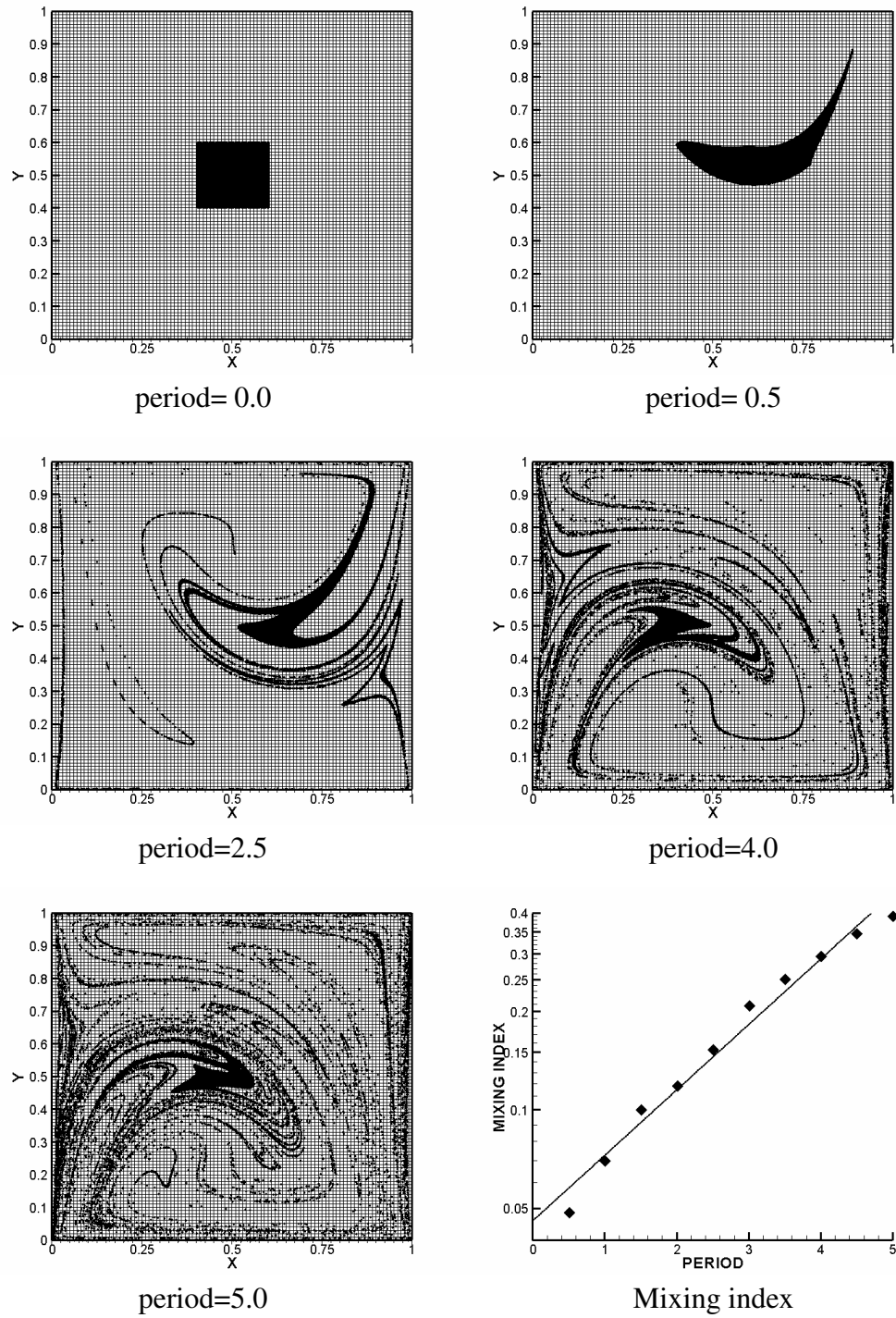


Figure 6-5. $T=10.0$, 20000 particles

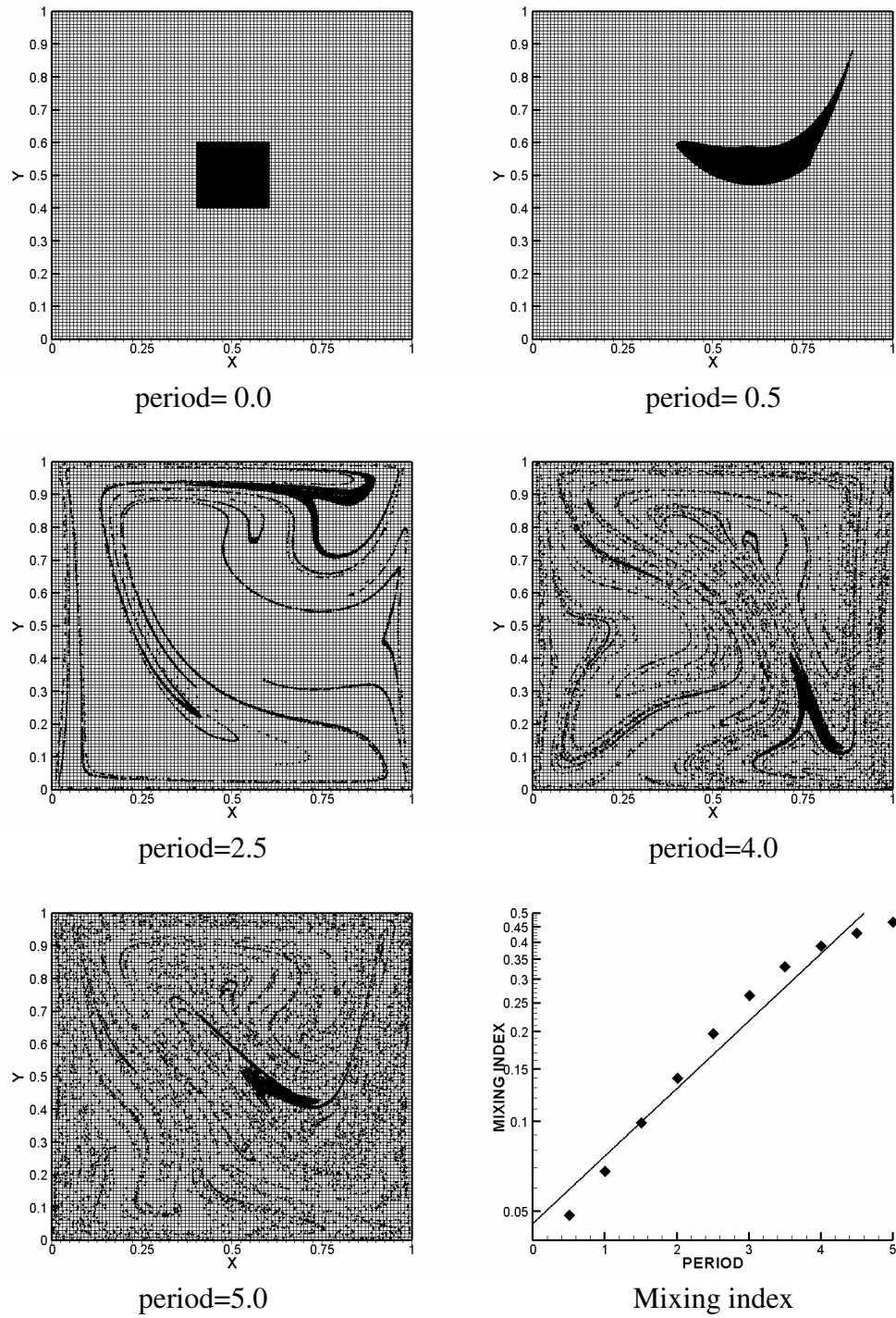


Figure 6-6. T=11.0, 10000 particles

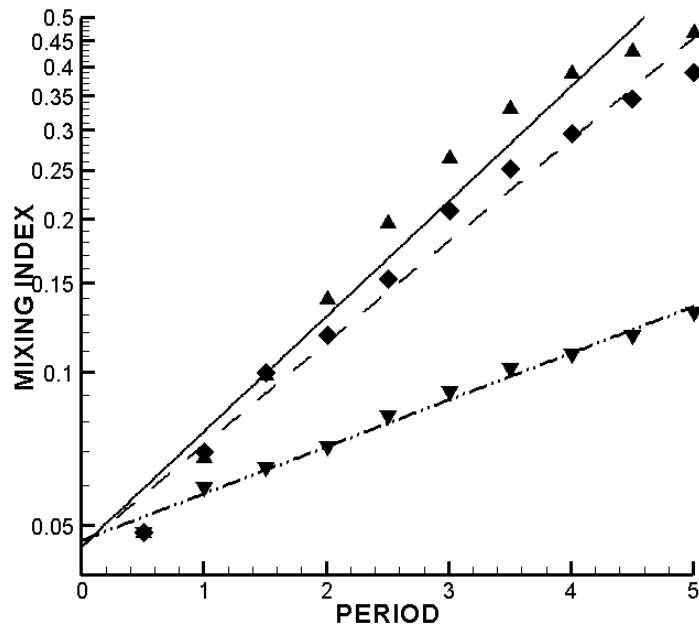


Figure 6-7. Comparison of mixing index :Gradient symbol : steady case (regular stirring), Diamond symbol : unsteady case, T=10.0 (chaotic stirring), Triangular symbol : unsteady case, T=11.0 (chaotic stirring)

In Figure 6-8, 11, 14, the particles are located initially in the center of mixing zone and they are dispersed from initial positions. For all flows, particles initially are convected exponentially, but dispersing rate decreases as the cells are filled up with particles. Consequently, the time evolution of mixing index curves has leveled off in Figure 6-9, 10, 12, 13, 15, 16.

As we expected using Lyapunov exponent, the A and D pattern at $T=6.0$ case flow accomplishes only incomplete dispersing with just about 70% of the cells contained by particles due to presence of large islands. For the high frequency flow, particle motion is regular in almost the entire flow so that it is expected that small portion of cells are contained even after 20 period. After 10 period, pattern B and C at $T=6.0$ and 8.0 flows achieve at least 85 % cell coverage. But pattern A and D at $T=6.0$ flow achieves only 70 % cell coverage after even 20 period in Figure 6-9, 10. This order is exactly same with order in Lyapunov exponent, Poincaré section and line stretching. In previous sections, we expected islands presence and bad mixing effects due to KAM boundaries and low value of Lyapunov exponent using Poincaré section. In Figure 6-17, 18, we set the size of T equal to 6.0 and change only pattern. In this comparison, first case is derived by pattern A and D and second case is derived by pattern B and C. As we expected in previous chapters, B and C case shows much more efficient curve than A and D pattern case. After enough time steps, mixing index of A and D pattern case is still much lower than B and C pattern case.

In Figure 6-19, 20, even though the size of T in B and C pattern at $T=8.0$ flow is larger than size of T in B and C pattern at $T=6.0$ flow, the chaotic strength of first case is weaker than second case. This causes by the separated high-stretching region. In the

separated high-stretching region, particles penetrate and leave such regions slowly [27, 28, 29]. To decrease the size of separated region, the optimum frequency is required so that Lyapunov exponent is used to find such frequency as soon as possible.

Finally, in Figure 6-21, we put 10000 particles in the center of mixing zone, and these particle sets are consisted of two color groups - blue and red. In chapter 4, the bad mixing zone is remained in the center of bottom part when particles are advected by pattern B and C at $T=6.0$ flow. As we expected, the bad mixing zone is also located in the site that we found using Poincaré section. With these facts, we can conclude that the cells contained no particles are located inside the islands. And also we find that mixing index is independent on the number of particles because mixing index of 10000 particles case has same trend with 1600 particles case in Figure 6-22.

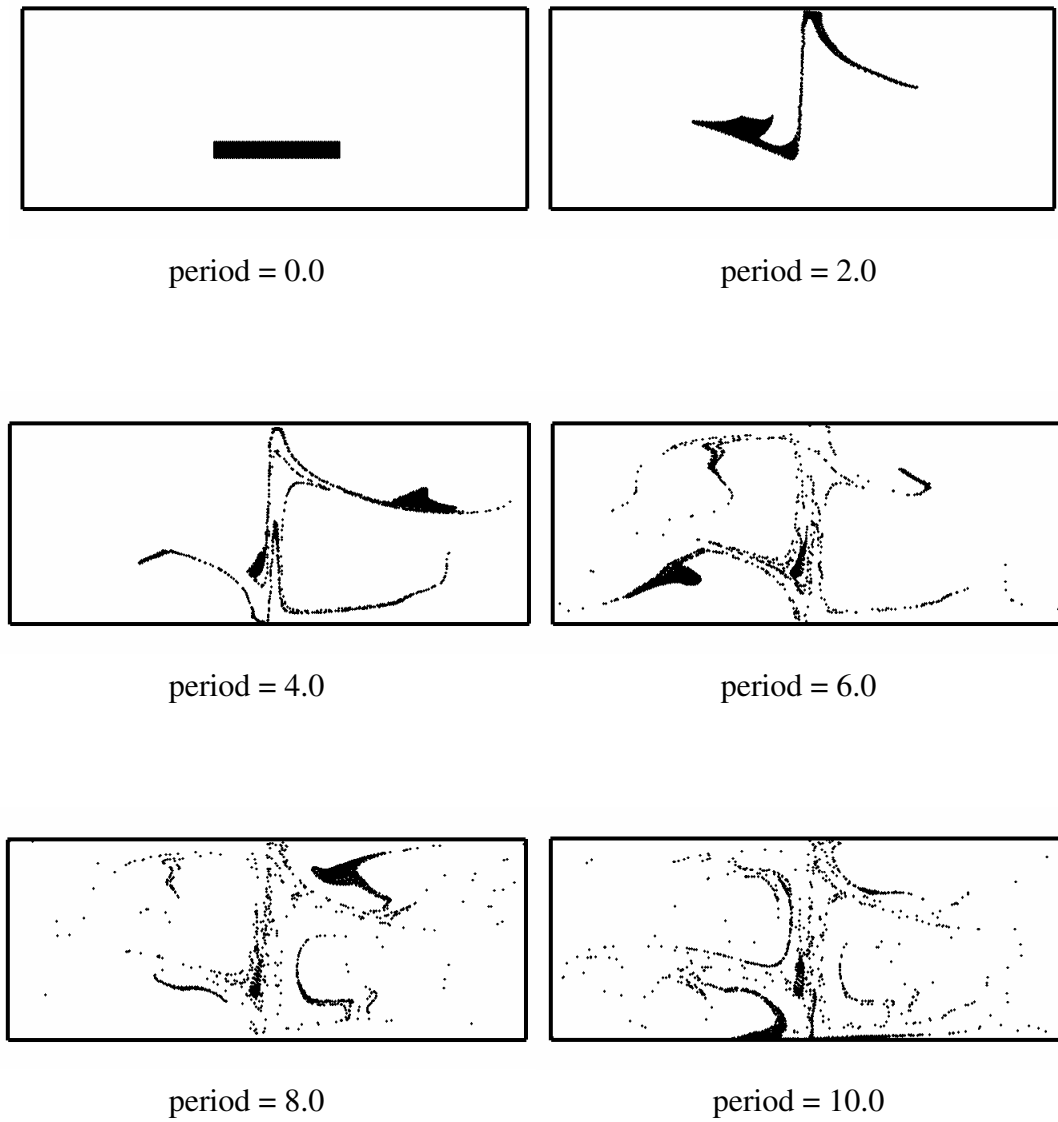


Figure 6-8. Snap shots of deformation of blob
A and D pattern : size of T = 6.0, 1600 particles

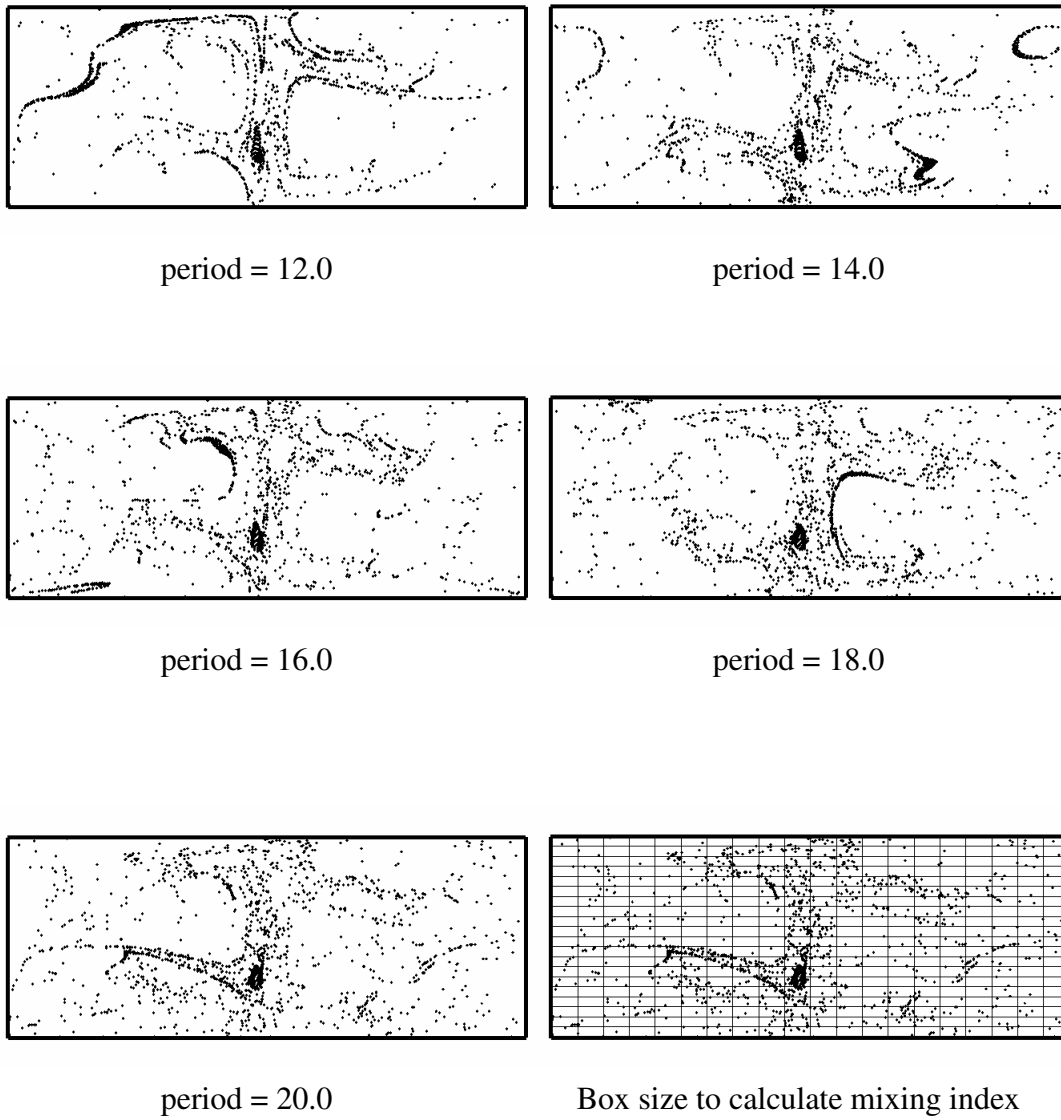


Figure 6-8. continued

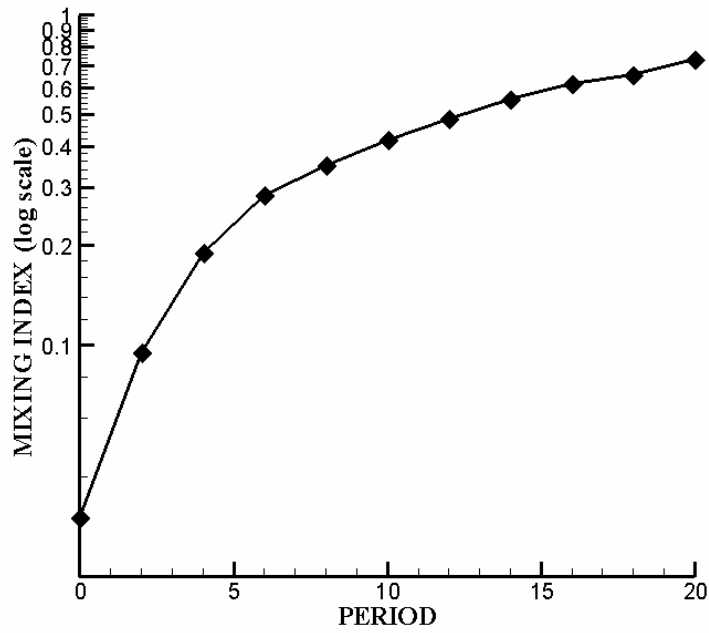


Figure 6-9. A and D pattern, size of $T = 6.0$, 1600 particles without concern of number of particles per box

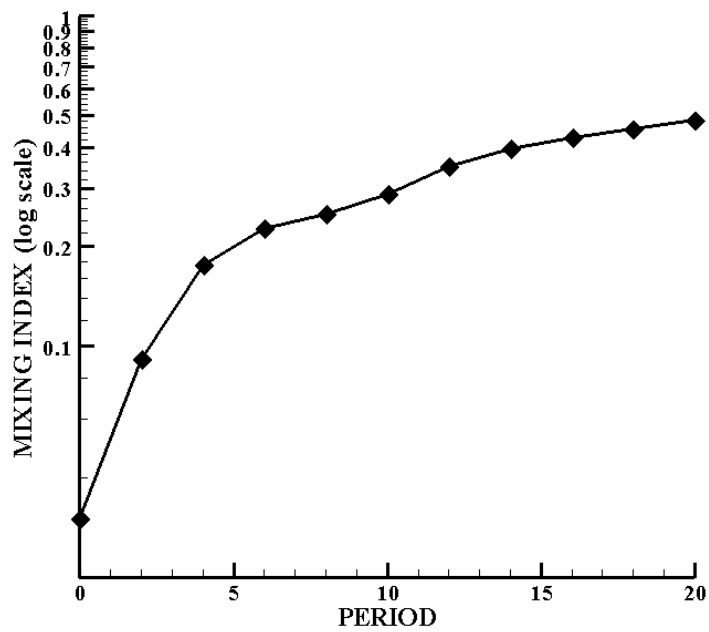


Figure 6-10. A and D pattern, size of $T = 6.0$, 1600 particles with concern of number of particles per box

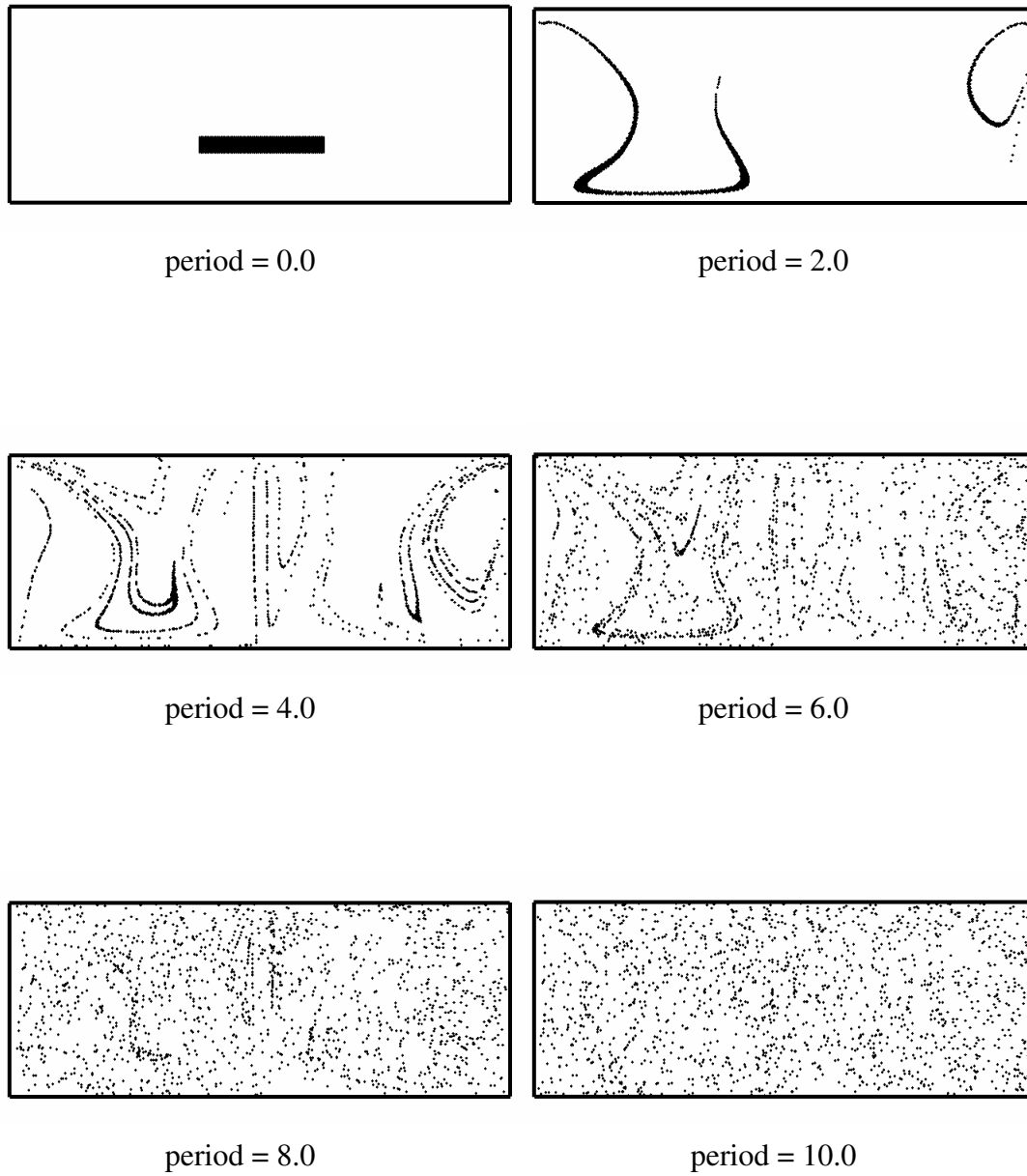


Figure 6-11. Snap shots of deformation of blob
B and C pattern : size of $T = 6.0$, 1600 particles

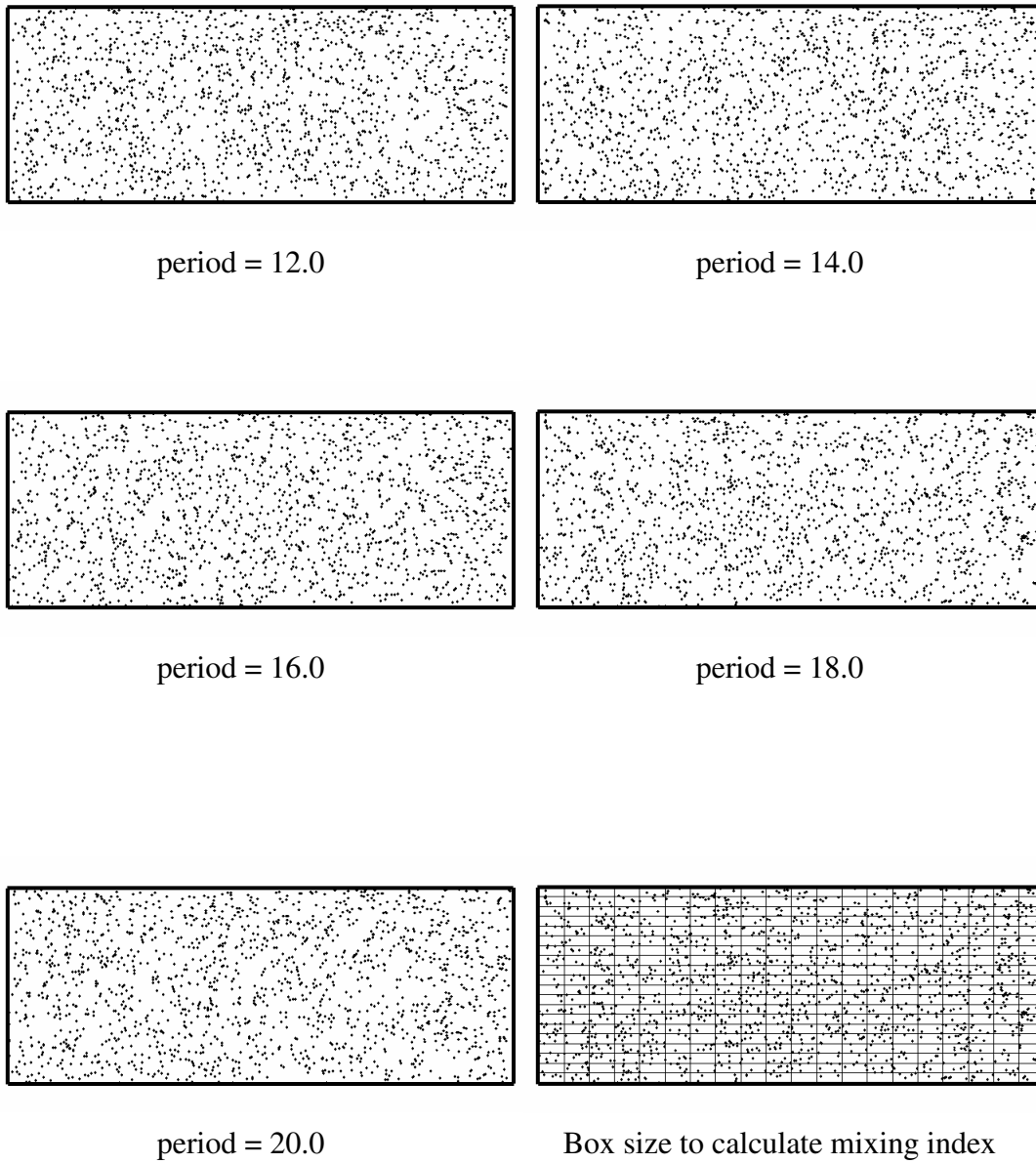


Figure 6-11. continued

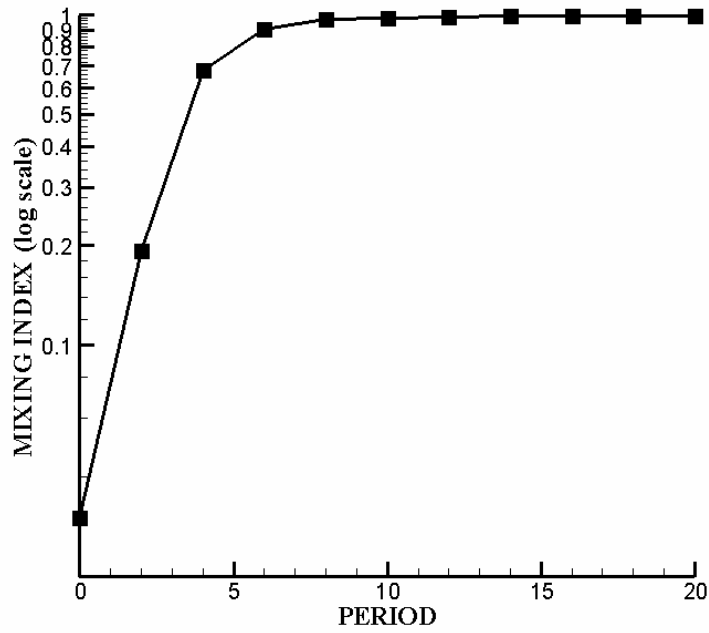


Figure 6-12. B and C pattern , size of $T = 6.0$, 1600 particles without concern of number of particles per box

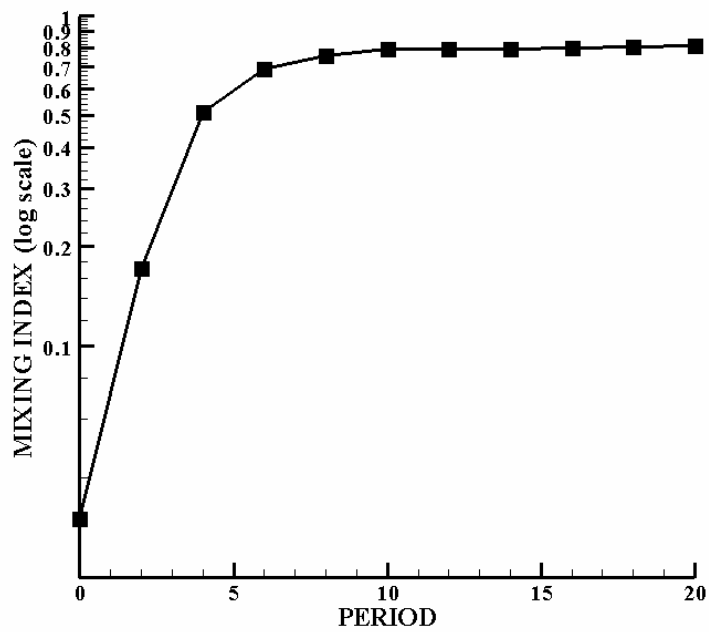


Figure 6-13. B and C pattern , size of $T = 6.0$, 1600 particles with concern of number of particles per box

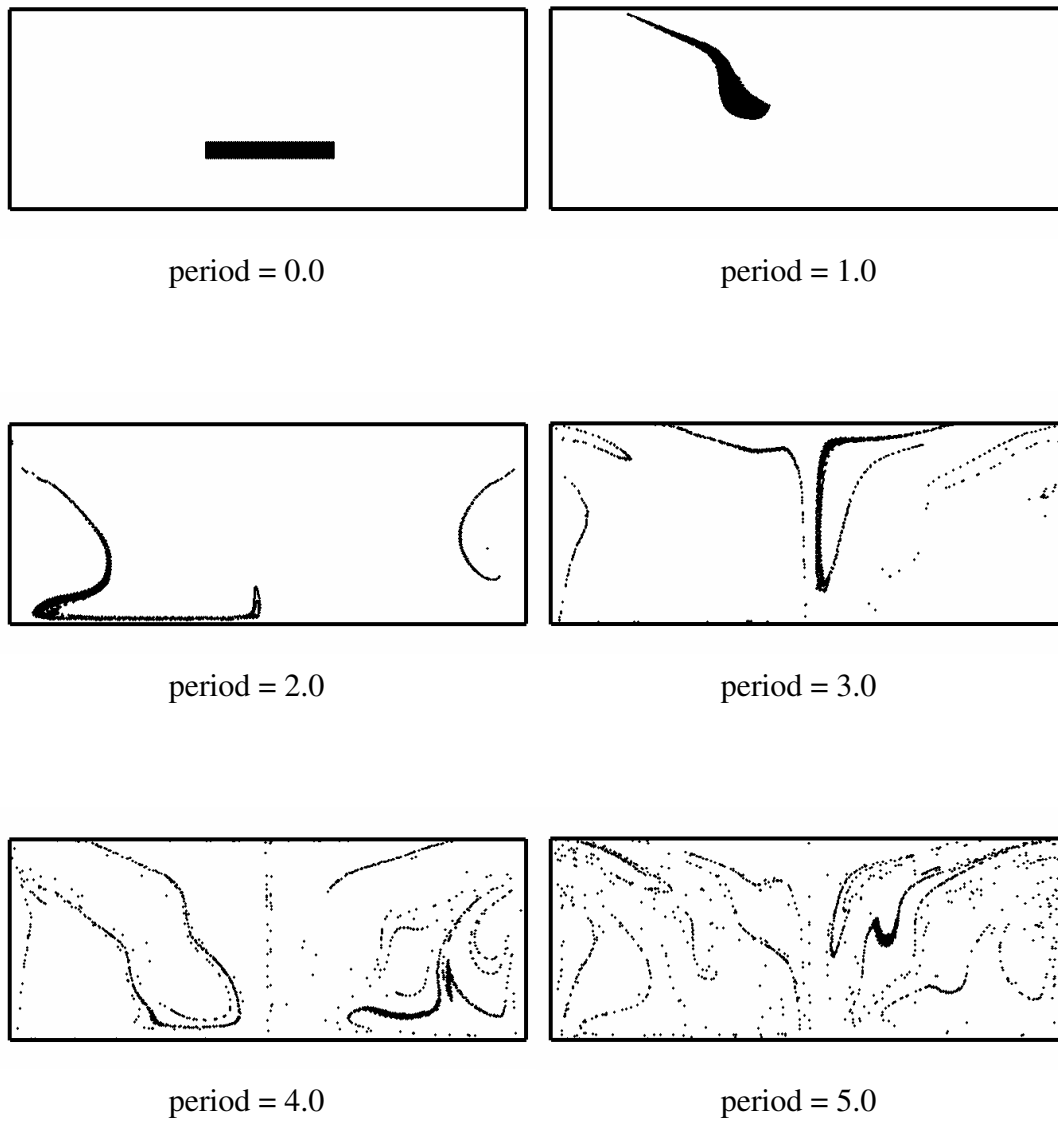


Figure 6-14. Snap shots of deformation of blob
B and C pattern , size of $T = 8.0$, 1600 particles

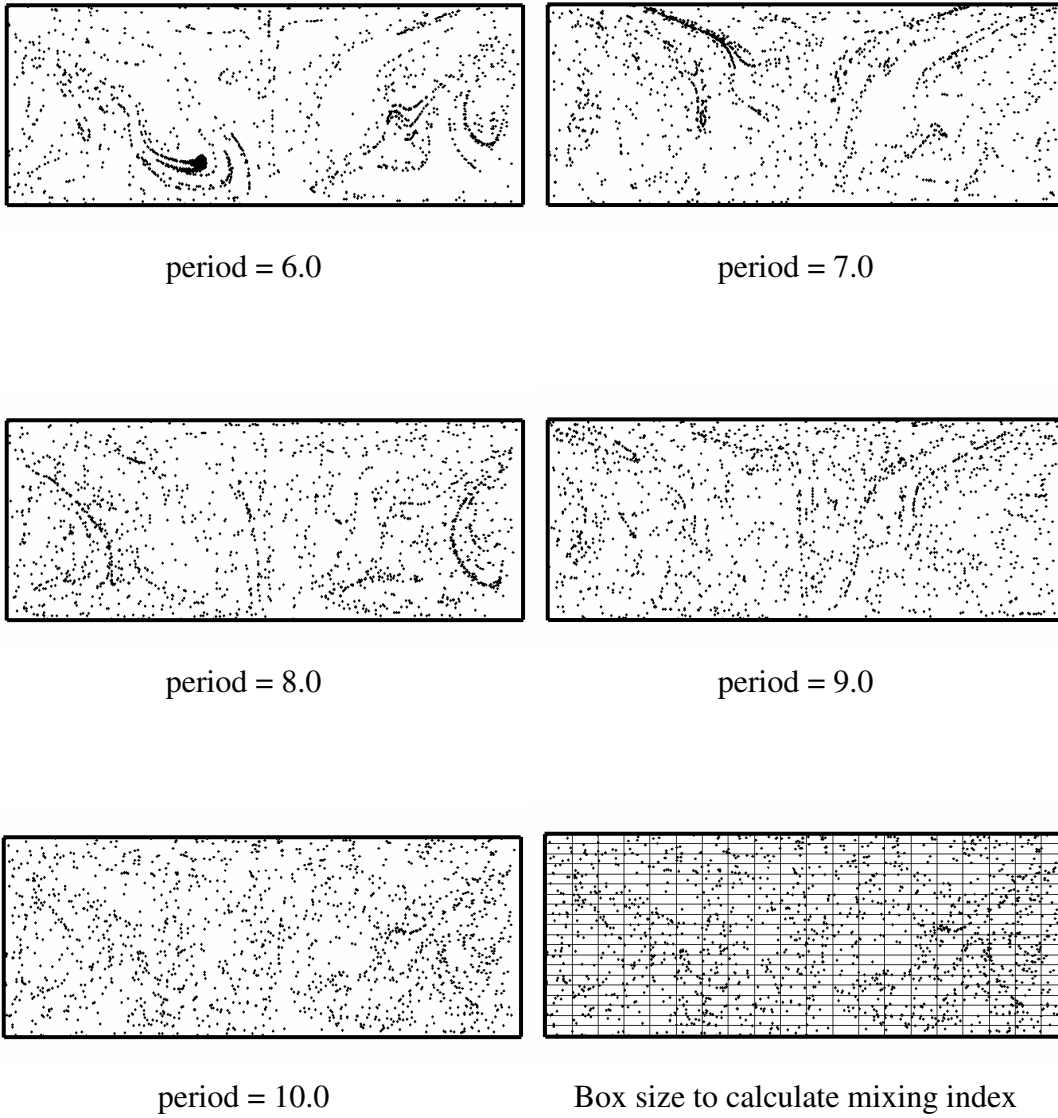


Figure 6-14. continued

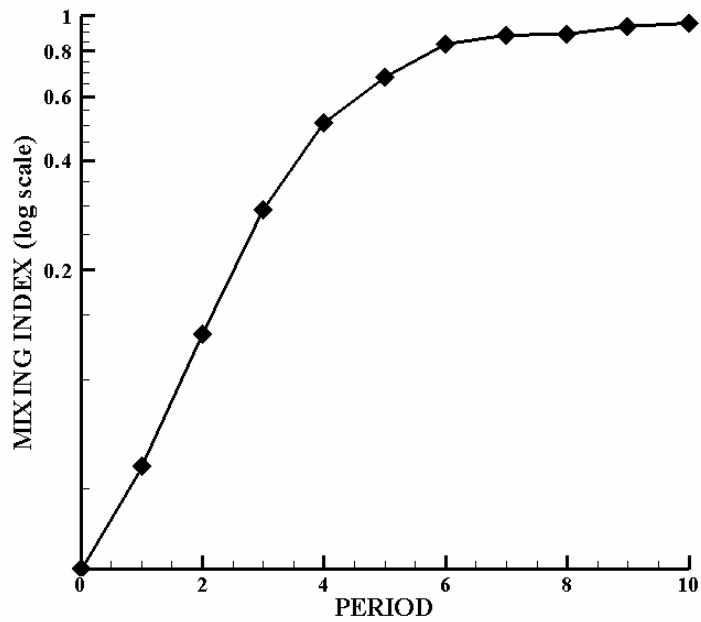


Figure 6-15. B and C pattern , size of $T = 8.0$, 1600 particles Mixing Index without concern of number of particles per box

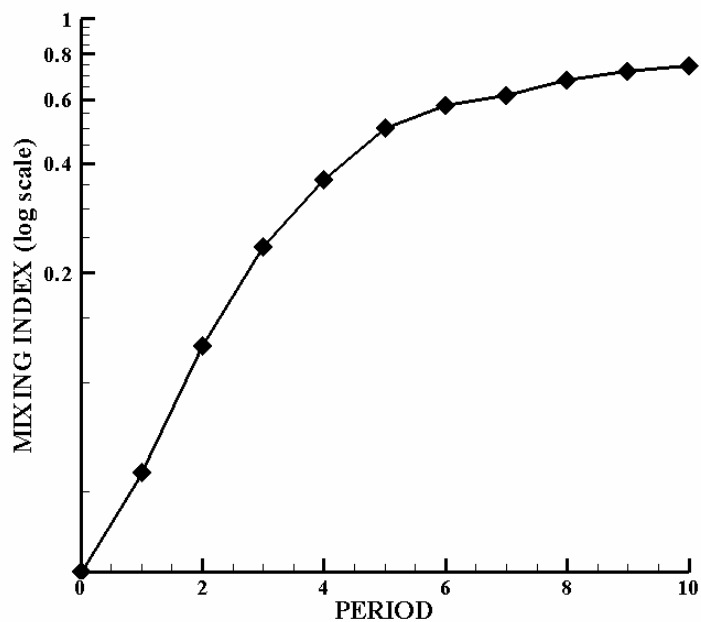


Figure 6-16. B and C pattern , size of $T = 8.0$, 1600 particles Mixing Index without concern of number of particles per box

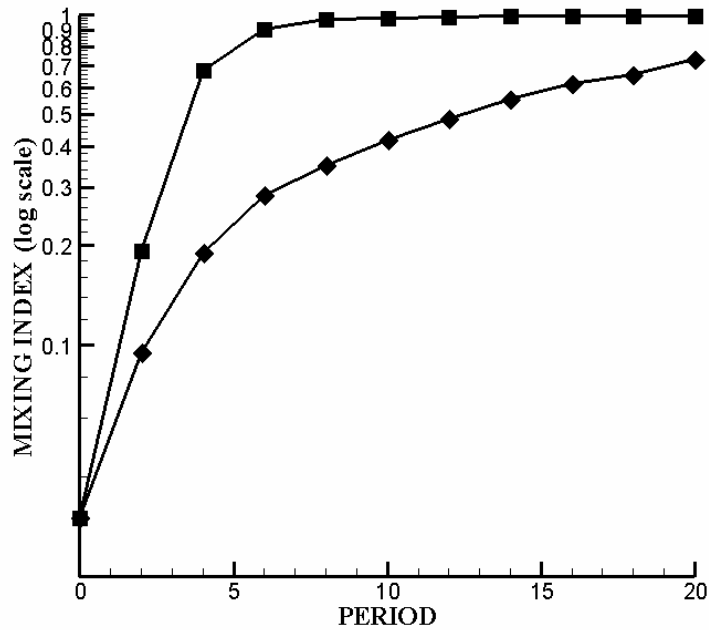


Figure 6-17. Comparison of Mixing Index between “B and C” and “A and D” (log - linear scale) : Without concern of number of particles per box, $T = 6.0$ fixed

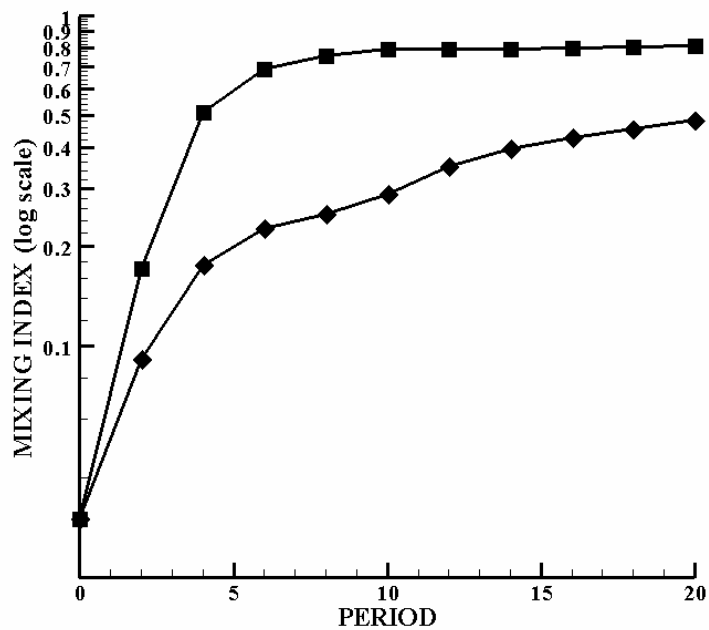


Figure 6-18. Comparison of Mixing Index between “B and C” and “A and D” (log - linear scale) : With concern of number of particles per box, $T = 6.0$ fixed

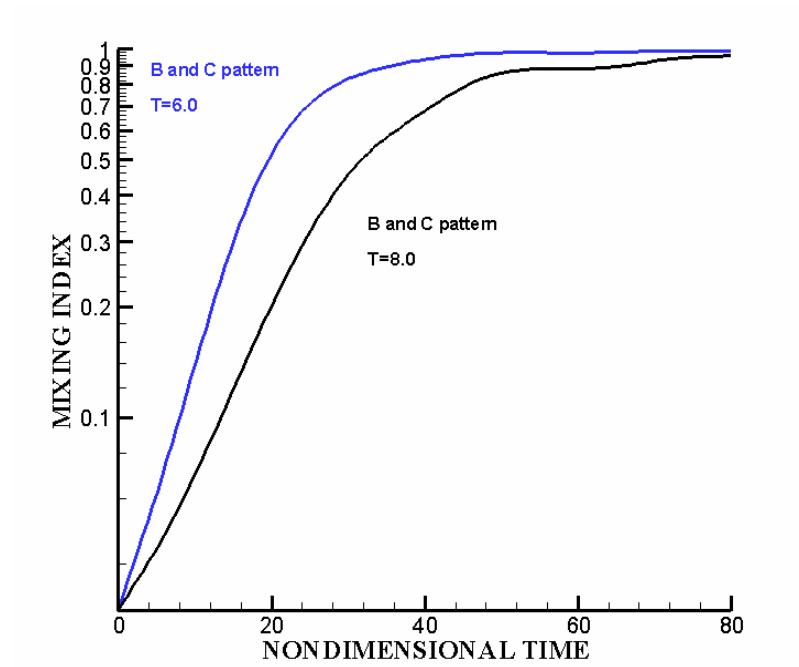


Figure 6-19. Comparison of Mixing Index between B and C T=6.0 and T=8.0 (log - linear scale) : Without concern of number of particles per box

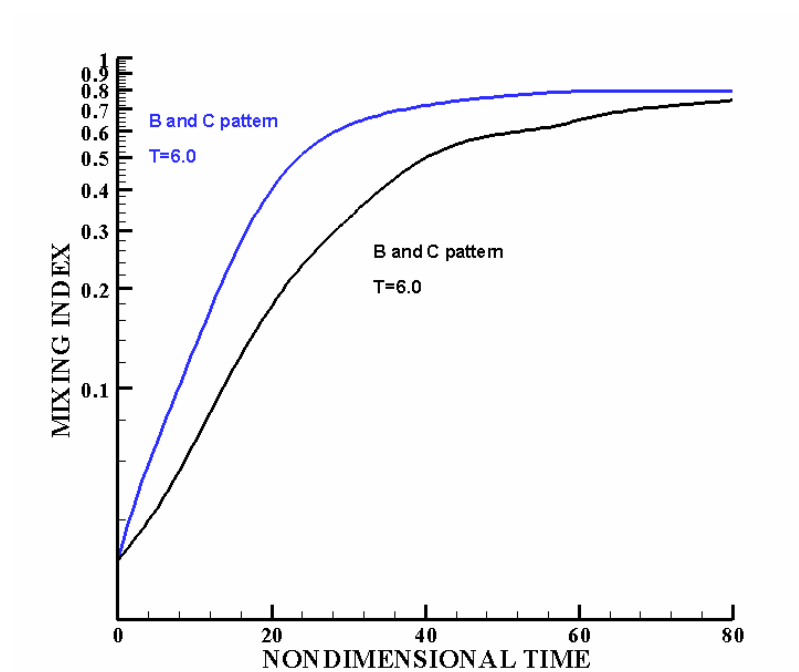


Figure 6-20. Comparison of Mixing Index between B and C T=6.0 and T=8.0 (log - linear scale) : Without concern of number of particles per box

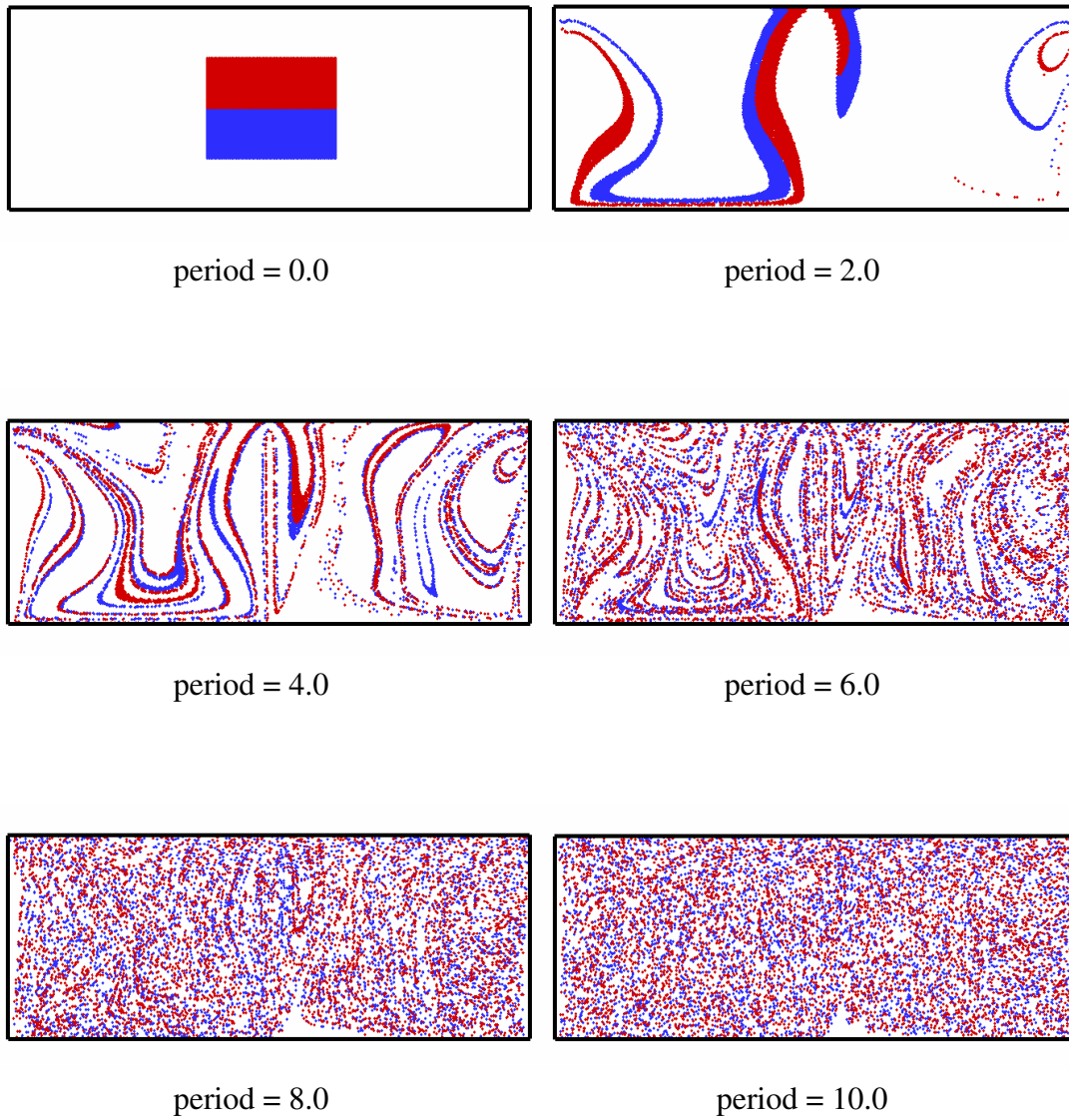
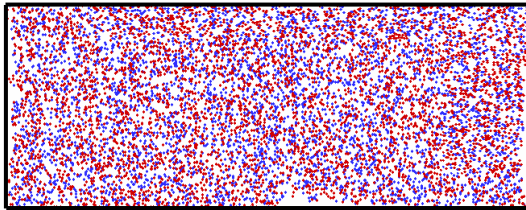
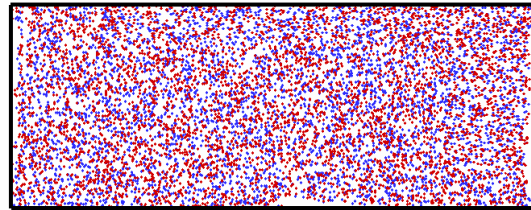


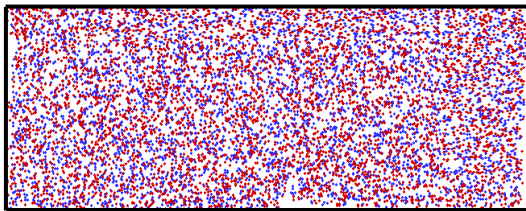
Figure 6-21. B and C pattern : size of $T = 6.0$, 10000 particles



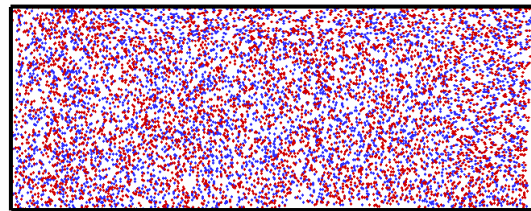
period = 12.0



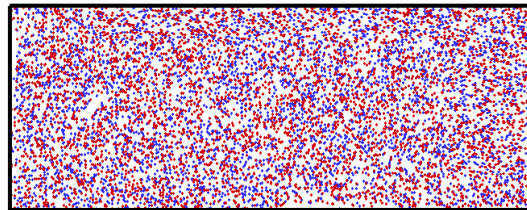
period = 14.0



period = 16.0



period = 18.0



period = 20.0

Figure 6-21. continued

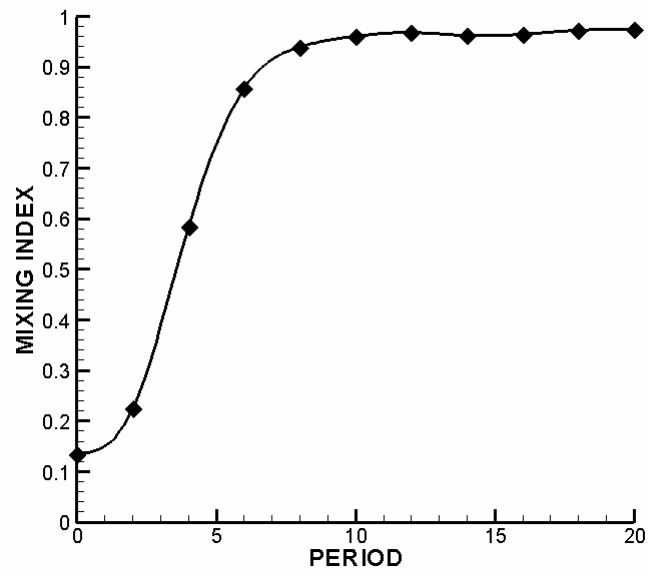


Figure 6-22. Mixing Index

CHAPTER VII

CONCLUSIONS AND FUTURE WORK

The main conclusions from our work are :

1. Chaotic mixing can result in very efficient mixing due to exponential interface stretching. Chaotic advection makes stretching rate grow exponentially. Consequently, mixing efficiency is enhanced.
2. Lyapunov exponent is defined as a quantitative measure of the sensitivity dependence on the initial conditions and the average rate of divergence (or convergence) of two neighboring trajectories. Lyapunov exponent measures efficiency of divergence of passive particles. If Lyapunov exponent is increased, the chaotic strength becomes stronger.
3. Graphical methods tell us usually more than the analytical solution so that we use 'map' and then try to make Poincaré section. In Poincaré section, destruction of KAM boundaries (islands) shows increasing chaotic strength. If system becomes fully chaotic, there are no islands any more in Poincaré section.
4. Length of interface was stretched exponentially in chaotic mixing. However, interface may lose its coherence as particles are dispersed. So we should carefully consider when length of stretching is physical and reasonable.
5. Box counting method gives quantitative measure of mixing quality. For chaotic state, mixing index grows exponentially.

In regards to the future work, we recommend that

1. Computing diffusion case using numerical simulation
2. Applying 3 dimensional steady case
3. Applying 3 dimensional unsteady case
4. Implementing inertial particle case [29, 30, 31]
5. Quantifying Poincaré section for general usages [32, 33, 34, 35, 36, 37]
6. Calculating striation thickness using probability density function

REFERENCES

- (1) Aref, H. *J. Fluid Mech.* **1984**, *143*, 1-21.
- (2) Aref, H. ; Balachandar, S. *Phys. Fluids* **1986**, *29(11)*, 3515-3521.
- (3) Strook, A. D. ; Dertinger, S. K. W. ; Ajdari, A. ; Mezić, I. ; Stone, H. A. ; Whitesides, G. M. *Science* **2002**, *295*, 647-651.
- (4) Alligood, K. T. ; Sauer, T. D. ; Yorke, J. A., *Chaos : an introduction to dynamical systems*, Springer ; New York ; 1997.
- (5) Qian, S. ; Bau, H. H. *Anal. Chem.* **2002**, *74*, 3616-3625
- (6) Jones, S. W. *Chaotic advection and dispersion*, TAM report, Department of Theoretical and Applied Mechanics ; University of Illinois, Urbana Champaign.
- (7) Beskok A., Karniadakis G. M. *Micro flows – fundamentals and simulation*, Springer ; New York ; 2001.
- (8) Wolf, A. ; Swift, J. B. ; Swinney, H. L. ; Vastano, J. A. *Physica D* **1985**, *16*, 285-317.
- (9) Ling, F. H. ; Schmidt, G. *Physics Letters A* **1992**, *165*, 221-230.
- (10) Niu, X. ; Lee, YK. *J. Micromech. Microeng.* **2003**, *13*, 454-462.
- (11) Sprott, J. C., *Calculation of Largest Lyapunov Exponent*, <http://sprott.physics.wisc.edu/>
- (12) Suzuki, H. ; Nakano, M. ; Kasagi, N. ; HO, CM., *Particle tracking velocimetry measurement of chaotic mixing in a micro mixer*, The International Symposium on Micro-mechanical Engineering, Japan, December 1-3, 2003.
- (13) Tsega, Y. ; Michaelides, E. E. ; Eschenazi, E. V. *Chaos* **2001**, *11*, 351-358.

- (14) Wiggins, S., *Introduction to applied nonlinear dynamical systems and chaos*, Springer-Verlag, New York, 1990.
- (15) Anderson, P. D. ; Galaktionov, O. S. ; Peters, G. W. M. ; Vosse, F. N. ; Meijer, H. E. H. *International Journal of Heat and Fluid Flow* **2000**, 21,176-185.
- (16) Anderson, P. D. ; Galaktionov, O. S. ; Peters, G. W. M. ; Vosse, F. N. ; Meijer, H. E. H. *J. Fluid Mech.* **1999**, 386, 149-166.
- (17) Ottino, J. M., *The kinematics of mixing : stretching, chaos, and transport* ; New York : Cambridge University Press, 1989.
- (18) Drakos, N., *Lecture of chaos*, <http://www.astro.cf.ac.uk/undergrad/module/PX3230/04>. **2004**
- (19) Tabor, M. ; Klapper, I. *Chaos, Solitons & Fractals* **1994**, 4 (6), 1031-1055.
- (20) Muzzio, F. J. ; Swanson, P. D. ; Ottino, J. M. *Phys. Fluids A* **1991**, 3 (5), 822-834.
- (21) Nishimura, T. ; Kunitsugu, K. *Int. J. Heat and Fluid Flow* **1997**, 18, 497-506.
- (22) Tan, B. T. ; Morris, P. ; Thompson, M. C. ; Hourigan, K. *Applied Mathematical Modeling* **1998**, 22, 1047-1057.
- (23) Truesdell, R. A. ; Vorobieff, P. V. ; Sklar, L. A. ; Mammoli, A. A. *Physical Review E* **2003**, 67.
- (24) Gobby, D. ; Angeli, P. ; Gavriilidis, A. *J. Micromech. Microeng.* **2001**, 11, 126-132.
- (25) Liu, M. ; Muzzio, F. J. ; Peskin, R. L. *Chaos, Solitons & Fractals* **1994**, 4 (6), 869-893.
- (26) Jones, S. W. *Phys. Fluids A* **1991**, 3 (5), May, 1081-1086.
- (27) Aubin, J. ; Fletcher, D. F. ; Bertrand, J. ; Xuereb, C. *Chem. Eng. Technol.* **2003**, 26 (12), 1262-1270.

- (28) Müller, S. D. ; Mezić, I. ; Walther, J. H. ; Koumoutsakos, P. *Computers & Fluids* **2004**, 33, 521-531.
- (29) Oddy, M. H. ; Santiago, J. G. ; Mikkelsen, J. C. *Anal. Chem.* **2001**, 73, 5822-5832.
- (30) Santiago, J.G. *Anal. Chem.* **2001**, 73 (10), May 15, 2353-2365.
- (31) Devasenathipathy, S. ; Santiago, J. G. ; Takehara, K. *Anal. Chem.* **2002**, 74, 3704-3713.
- (32) Lorenz, E. N. *Journal of the Atmospheric Science* **1963**, 20, 130-141.
- (33) Theiler, J. *J. Opt. Soc. Am. A.* **1990**, 7 (6), 1055-1073.
- (34) Farmer, J. D. ; Ott, E. ; Yorke, J. A.. *Physica D* **1983**, 7, 153-180.
- (35) Grassberger, P. *Physics Letters* **1983**, 97 A (6), 227-230.
- (36) Falconer, K. *Fractal Geometry, Mathematical Foundations and Applications*, John Wiley & Sons : Chichester, U.K., 1990.
- (37) Peitgen, H. ; Jürgens, H. ; Saupe, D., *Chaos and Fractals*, Springer: Berlin, 2003.

VITA

Ho Jun Kim was born in Seoul, South Korea. He attended Hanyang University between 1998-2002 and received his B.S. in mechanical engineering. He began graduate school in the Fall of 2002 at Texas A&M University. He joined the research group of Dr. Ali Beskok in the Fall of 2003. His technical interests are in computational fluid dynamics, chaos theory, Lagrangian particle transport.

Ho Jun Kim can be reached at hojunkim@neo.tamu.edu. His permanent address is: Jookong Apt.138-201, Joongang-dong, Kwacheonsi, Kyoungkido, South Korea, 427-010.